A 3D *In Vitro* Ring Model with Macrophage and Fibroblast Co-culture: A Platform for Preclinical Fibrosis Studies as an Alternative to Animal Testing

By Yaunghyun Kim

B.S. Massachusetts College of Pharmacy and Health Sciences, 2022

Thesis

Submitted in partial fulfillment of the requirements for the Degree of Master of Science

in the Graduate Program of Biotechnology at Brown University

This thesis by Yaunghyun Kim is accepted in its present form by the Graduate Program in Biotechnology as satisfying the thesis requirements for the degree of Master of Science

Date _____ Signature:_____

Dr. Jeffrey Morgan, Advisor

Date _____ Signature:_____

Dr. Theresa Raimondo, Co-Advisor

Date _____ Signature:_____

Dr. Adam Crego, Reader

Approved by the Graduate Council

Date _____ Signature:_____

Dr. David P. Lindstrom, Dean of the Graduate School

Acknowledgement

I would like to express my sincere gratitude to my principal investigators, Dr. Jeffrey Morgan and Dr. Theresa Raimondo, for their unwavering support, guidance, and encouragement throughout my research journey. Their expertise and vision greatly shaped this work, and I am truly grateful for the opportunities they provided me. I would also like to thank Madeleine Marx for endless help in generating confocal images and Katerina St. Angelo, Nicholas Nocevsk, Angelina Schorr, and Wuyi Zhang for various support. I would like to express appreciation to all current and former members of the Morgan Lab and the Raimondo Lab for their collaboration, insights, and support mentally and academically. Their contributions made this experience both enlightening and enjoyable, and I appreciate each one of them for their support. A heartfelt thank you goes to my family, whose love and encouragement have been my foundation. Your belief in me kept me motivated during the challenging moments. Lastly, I would like to acknowledge my friends, who offered invaluable mental support throughout this process. Your constant encouragement and companionship have been a source of strength for me. Thank you all for being an integral part of this journey.

Table of Contents

Table of Figures

S2. *x, y*- and *z*- thickness measurements and statistical analysis on each macrophage phenotype-myofibroblast 1:16 co-culture rings.

S3. *x, y*-dimensional image of each macrophage phenotype to myofibroblast.

Abstract of A 3D In Vitro Ring Model with Macrophage and Fibroblast Co-culture: A Platform for Preclinical Fibrosis Studies as an Alternative to Animal Testing, by Yaunghyun Kim, ScM., Brown University, May 2026

Abstract

This study presents a scaffold-free 3D ring-shaped co-culture model composed of human dermal fibroblasts and THP-1 monocyte-derived macrophages to recapitulate cellular interactions associated with tissue fibrogenic conditions more closely. We optimized the 50:50 culture medium and established a macrophage-to-fibroblast ratio of 1:16 as the most ring-structured, stable culture setting with M0 macrophages. With M1 and M2 co-culture in optimized settings, significant contraction in the *x, y*- plane from day 2 was observed onward compared with the fibroblast-only control. In contrast, the addition of M1 macrophages led to a reduction in *x, y*-thickness starting from 24 hours post-seeding.

To examine variations in immunological roles in tissue morphology, proinflammatory M1 and profibrotic/anti-inflammatory M2a and M2c were observed in the *x, y-,* and *z*-dimensions until day 7. To assess biochemical changes, we measured P1CP levels in the supernatants of each co-culture model to evaluate relative collagen production over time. Profibrotic M2a macrophage rings secreted the highest level of P1CP, suggesting the most fibrogenesis effect on fibroblast cells at an early stage. Proinflammatory M1 macrophages increased collagen production at later time points, suggesting potential activation of the profibrotic process through a non-canonical pathway activation by the inflammatory cytokine. Due to macrophages' high plasticity, we visualized the M1, M2a, and M2c phenotypes by immunostaining for CD86, CD206, and CD163 using fluorescent immunohistochemistry. Myofibroblast activation was also assessed in different macrophage co-cultures using αSMA staining. The reduced activation of myofibroblasts was associated with a reduction in collagen production across later time points in M2 co-cultured

rings and myofibroblast-only rings. In contrast, prolonged myofibroblast activation in M1 co-cultured rings demonstrated a correlation with increased collagen production towards later time points. These findings demonstrate the potential of this 3D *in vitro* platform as a physiologically relevant and quantifiable alternative to conventional 2D culture, 3D spheroids, and animal models for studying fibrosis induced by macrophage-fibroblast crosstalk and for evaluating therapeutic intervention.

Introduction

Fibrosis is a global burden that contributes to nearly half of all deaths in industrialized countries as a pathological condition.[1] Approximately 4,968 per 100,000 person-years are fibrosis-related disease incidents, accounting for 16.71% of global disability-adjusted life-years (DALYs) in the Global Burden of Disease (GBD) 2021 database.[1,2] Including cancer-associated fibrosis (CAF) conditions, the overall contribution to global mortality was 28.7% in 1990 and steadily rose to 35.4% in 2019 in the 2019 GBD database.[3] Currently, there are three FDA-approved drugs available for idiopathic pulmonary fibrosis (IPF). All three anti-fibrotic therapies slow progression rather than cure and reprogram the fibrogenic condition back to normal. However, slow progression without reversing, the disease state can ultimately lead to organ failure, which is linked to high morbidity and mortality. [4] Additionally, the reason for high mortality and morbidity is due to the difficulty of detection and diagnosis during earlier stages, which is critical for patients' life expectancy. There is increasing recognition of fibrosis as a major health issue.

Fibrosis can occur in many organs, including the lung, liver, kidney, heart, and skin, by forming excessive deposits of fibrous connective tissue and extracellular matrix (ECM) after injury. Fibrogenesis is a dysregulation of normal wound healing that can occur in damaged tissue. At the site of damage, active inflammation promotes the accumulation of neutrophils, eosinophils, and macrophages, along with upregulated inflammatory mediators, to clear debris and necrotic areas. Activated fibroblasts and other mesenchymal cells transform into myofibroblasts.[2] Under normal conditions, myofibroblasts play a crucial physiological role in the rapid repair of injured tissues and are cleared from wounded sites via apoptosis to restore tissue

homeostasis.[2,5,6] However, when programmed cell death fails and if myofibroblasts are chronically activated, they persistently secrete ECM components, including collagens, fibronectin, and hyaluronic acid. Chronic myofibroblast activation leads to increased stiffness at the scarred area beyond the limits of normal repair, disrupting oxygen diffusion, causing cellular damage, decreased organ function, organ failure, and, ultimately, death.[2,6,7] Therefore, a key effector cell in fibrosis is the myofibroblast, which is activated from fibroblasts by chemical or mechanical stimuli.[7]

At fibrotic foci (FF), epithelial cells, endothelial cells, and fibroblasts are the main structural cells affected by responders, such as innate immune cells and progenitor cells. Immunocytes, including T lymphocytes, natural killer (NK) cells, macrophages, dendritic cells, granulocytes, and mast cells, are involved in fibrogenesis at all stages, accompanied by innate and adaptive immune responses. [2,5] As a first-line defense, innate immune responses are initiated by macrophages, neutrophils, NK cells, and dendritic cells, leading to the recruitment and differentiation of circulating and resident monocytes into macrophages and dendritic cells.[5] However, elevated monocyte counts were associated with a worse prognosis in IPF patients, leading to increased hospitalizations and mortality.[8] Monocyte-derived macrophages are known to be more important drivers of fibrosis than resident macrophage cells.[5,9]

There are two main subsets of macrophage cells. Pro-inflammatory M1 macrophages are activated by IFN-γ, TNFα, GM-CSF, or lipopolysaccharide stimulation. M1 are the main source of upregulation and secretion of inflammatory cytokines such as IL-1β, IL-6, IL-12, TNFα, and CXCL10, which induce further polarization of M1 macrophages via a positive feedback. [9–11] In contrast, M2 macrophages are anti-inflammatory and are activated by stimuli of IL-4, IL-10, IL-13, and TGF-β. M2 macrophages are tissue-repairing phenotypes that produce various growth

factors, including TGF-β, fibroblast-derived growth factor (FGF), platelet-derived growth factor (PDGF), and vascular endothelial growth factor (VEGF) (Table 1). M2 macrophages are known to be a key effector cell in fibrosis via upregulated inflammatory and fibrotic cytokines, which trigger the activation of fibroblasts into myofibroblasts through paracrine and autocrine signaling pathways. Major growth factors and their associated signaling pathways that promote fibrosis by activating fibroblasts include TGF-βs, PDGFs, FGFs, and connective tissue growth factors (CTGFs), with downstream signals including phosphatidylinositol 3-kinase (PI3K)/protein kinase B (AKT), JAK/STAT, and WNT/β-catenin.[2] However, the detailed underlying mechanisms of fibrosis induced by macrophages and the stimuli driving M2 polarization from the initial inflammatory response in the fibrosis area are very complex and have not been fully elucidated.

Fibrogenesis is induced by an activated TGF-β intracellular pathway, which triggers canonical and non-canonical signaling cascades that regulate myofibroblast generation, fibroblast proliferation/apoptosis, and ECM protein production.[12] The canonical pathway is the fibrosis signaling pathway via SMAD2/3. When the TGF-β ligand binds to the TGF-β type II receptor, it induces phosphorylation and activation of TGF-β receptor type I. Activated TGF-βRI activates SMAD2/3 protein to recruit and form a complex with SMAD4. This complex translocates into the nucleus and interacts with DNA by transcription factor, co-activators, and co-repressors to regulate gene expression which alters increased expression of alpha-smooth muscle actin (αSMA), epithelial-mesenchymal transition (EMT), excessive ECM production such as collagen production, cell proliferation, suppression of matrix degradation, and increased pro-fibrotic factor connective tissue growth factor (CTGF) to promote fibrosis.[12–14] While the canonical SMAD2/3 cascade is central to organ-specific fibrogenesis, SMAD-independent non-canonical

cascades such as PI3K/AKT/mTOR, RhoA/ROCK, MKK/JNK, MKK/P38, MAPK/ERK and others activated by TGF-βR1 also regulate fibrosis either independently or cooperatively with SMAD signaling.[14,15] (Figure S4)

Among non-canonical SMAD-independent signaling pathways, JAK/STAT is also closely linked to macrophages, and interleukin and growth factor receptors activate it. When inflammatory cytokines such as IL-4, IL-6, IL-11, IL-13, and IL-31, and growth factors such as TGF-β, PDGF, VEGF, EGF, and FGF bind their receptors, receptor-coupled JAKs phosphorylate STATs. STATs enter into the nucleus and initiate gene transcription, leading to fibrosis via fibroblast differentiation, EMT, senescence, autophagy, and ERS (Figure S4).[12,15]

To study paracrine, autocrine, and juxtacrine signaling pathways of fibrogenesis and macrophage activation in M1 and M2 phenotypes, and their effects on myofibroblast activation, ultimately leading to fibrosis, various 2D and 3D culture models have been investigated. For example, 2D conditioned medium culture, direct co-culture or indirect co-culture, 3D organoid, 3D scaffold hydrogel, and 3D scaffold-free spheroid co-culture were widely used in studies of fibrosis to examine cellular crosstalk between macrophages and fibroblasts. However, a 2D monolayer has limitations for mimicking a 3D microenvironment *in vivo*, whereas a 3D scaffold hydrogel does not allow direct cell-cell contact. Therefore, 3D scaffold-free spheroids and organoid models are considered better mimics of the physiological microenvironment. However, a study by Tan Yu et al. demonstrated that 3D spheroid models have limitations in growing beyond 300 μm, as progressive apoptosis in the core is driven by hypoxia.[16]

To overcome the limitations of models used to mimic the fibrotic microenvironment, a 3D *in vitro* ring-shaped tissue co-culture was investigated in this study. Unlike 3D scaffold-free spheroids, our ring-shaped tissue provides a more defined geometry, enables more controlled

analysis of macrophage-fibroblast interactions, provides better diffusion gradients and a broader, steadier environment than the sole core of a spheroid. A ring model allows for measurement of the rings' mechanical properties. This thesis demonstrates the methodology for fabricating 3D ring-shaped tissue containing M1-polarized macrophages and M2-polarized macrophages with fibroblasts, in a 1:16 ratio. Among M2 subtypes, pro-fibrotic M2a and M2c were studied. Ratio and culture medium-dependent ring-structure retention was quantified with M0 macrophages for further study with M1 and M2s. Cell viability between culture media was optimized. To analyze the fibrogenesis effect between M1 and M2 macrophages, collagen synthesis was measured by P1CP ELISA. Characterization of cell differentiation and polarization at each time point was performed by immunostaining. Finally, the future direction of this study is to be further developed for potential use as a pre-diagnostic and drug-treatable model for fibrosis research, as demonstrated in this thesis.

Cell Type	Cytokines and growth factors secreted	Signaling pathway on fibroblasts
M1 macrophage	TNFα, IL-6, IL-12, IL-1β, IL-27, IL-23, CCL2, MMP-2 MMP-9, CXCL9, CXCL10, and CXCL11	JAKs
M2	IL-10, IL-4, IL-5, IL-13, IL-1β, CCL17, CCL18, CCL22, CCL24, TGF-β, FGF, PDGF	NKT/Th2, IL4/IL-13, JAKs
M2a macrophage	IL-10, TGF-β, CCL17, CCL18, CCL22	JAK/TYK/STAT, SMADs
M2c macrophage	IL-10, TGF-β, CCL16,	JAK/TYK/STAT, SMADs
Myofibroblast	IL-1α and β, IL-6, IL-10, TNFα, TGF-β	JAKs, SMADs

Table 1. Cytokines, chemokines, and growth factors secreted by macrophage phenotypes and fibroblasts, and their related signaling pathways. M1 and M2 macrophages secrete cytokines, chemokines, and growth factors that alter fibrogenesis. M1 are pro-inflammatory macrophages that secrete anti-inflammatory cytokines, which activate the JAK/STAT pathway, which can activate fibroblasts to myofibroblast transformation (FMT). There are 4 subtypes of M2 macrophages; however, M2a and M2c are investigated in this study due to their profibrotic characteristics, as they secrete TGF-β and activate the TGF-β/SMADs pathway to promote FMT.[10,17,18]

Materials and Methods

Fabrication of scaffold-free agarose hydrogel

A protocol for a scaffold-free 2% weight-by-volume agarose mold that allows the fabrication of a ring-shaped 3D *in vitro* tissue was established by the Morgan Lab (Figure 1). Prealiquoted and autoclaved agarose (Fisher Scientific, Hampton, NH) in sterile phosphate-buffered saline (PBS) (Corning, Glendale, AZ) was melted in the microwave. 1.5 mL of the molten 2% w/v agarose was added to each well of the 24-well plate (Figure 1a). Autoclaved sterile stainless steel inserts and a holder that fits perfectly onto a 24-well plate (25-piece system) were designed in the Morgan lab. This molding system was placed on top of a 24-well plate pre-filled with 1.5mL 2% agarose (Figure 1b). This 25-piece mold system allows the fabrication of 24 agarose molds with a 5 mm-diameter peg (Figure 1c-d). After the agarose solidified, the inserts were removed and the solidified non-adhesive hydrogel gel (2% Agarose w/v) was equilibrated in serum-free Dulbecco's modified Eagle medium (DMEM) with high glucose (Gibco, Waltham, MA) with 1% antibiotic (Pennicillin-streptomycin; MP Biomedicals) at 37 °C, 10% CO_2 incubator for 1-24 hours for three times before use.

50:50 media preparation

50:50, validated in the Morgan Lab, is culture media optimized for the fabrication of uniform 3D ring-shaped microtissues. 50:50 is composed of 50% of SFM+ media and 50% of SFMA media. Serum-free media advanced (SFMA) is made of advanced Dulbecco's modified Eagle medium (Advanced DMEM, Cat. 12491015, Gibco, Waltham, MA) with the addition of 2 mM L-glutamax (100X) (Gibco, Waltham, MA) and 1% antibiotic(10,000 IU pen/mL, 10 mg

strep/mL) (MP Biomedicals, Irvine, CA). Serum-free media plus (SFM+) is made of DMEM with high glucose (1X) (Cat. 11965092, Gibco, Waltham, MA) supplements with 50 µg/mL L-proline, 0.1 mM 2-phospho-L-ascorbic acid trisodium salt, and 1% penn/strep. The final concentration of supplements of 50:50 was half the amount of additives added in each SFMA and SFM+ media with 1% antibiotics in total. The final mixture of SFMA and SFM+ was sterile filtered through a 0.22 µm pore membrane disposable filter. (Corning, Glendale, AZ) This medium is hereafter referred to as '50:50.'

Fibroblast 2D culture

Primary juvenile normal human dermal fibroblast (jNHDF) from PromoCell (Heidelberg, Germany) was passaged and subcultured in T-175 flasks with Dulbecco's modified Eagle medium high glucose + l-glutamine, phenol red, and sodium pyruvate (DMEM) (Cat. 11965092, Gibco, Waltham, MA) with 10% fetal bovine serum and 1% antibiotic (10,000 IU pen/mL, 10 mg strep/mL) (MP Biomedicals, Irvine, CA). The medium hereafter is referred to as 'complete DMEM.' Once fibroblasts reached 80% confluency, flasks were rinsed with PBS and trypsinized with 0.05% trypsin-EDTA protease (Cytiva, Wilmington, DE). Detached cells were centrifuged at 800 rpm for 6 minutes, and resuspended cells were then passed at 500,000 cells per flask. 300,000 cells per ring were centrifuged again to be reconstituted in 50:50 serum-free media to achieve a final concentration of 300,000 cells/75 µL cell solution upon seeding.

Myofibroblast differentiation

Primary jNHDF cells were passed and cultured in T-175 flasks, and 80% confluence occurred after 7 days in complete DMEM with media refresh every other day. To differentiate fibroblast

cells into myofibroblast, 10 ng/mL transforming growth factor beta 1 (TGF-β1) (Peprotech, Rocky Hill, NJ) was added 36 hr prior to cell detachment to be seeded into the agarose molds.

THP-1 monocyte culture

THP-1 cells, a human monocytic cell line derived from acute monocytic leukemia, were cultured in Roswell Park Memorial Institute medium (RPMI 1640; Corning, Glendale, AZ) supplemented with 2 mM L-glutamine (Gibco, Waltham, MA), 10 mM HEPES (Gibco, Waltham, MA), 1 mM Sodium Pyruvate (Gibco, Waltham, MA), 10% FBS, and 1% penn/strep cultured in T-25 or T-75 flasks at 5% CO_2, 37 °C. The cell culture media hereafter is referred to as 'complete RPMI.' Non-adherent THP-1 cells were centrifuged at 270 g for 8 minutes to refresh the media and maintained in complete RPMI at the desired cell density below 1,000,000 cells per mL for the best expansion and viability.

THP-1 monocyte differentiation into M0 macrophages

Due to a low yield of macrophage cells, 10 times the desired number of THP-1 monocytes were differentiated into M0 macrophage by the addition of a 200 ng/mL phorbol 12-myristate 13-acetate (PMA) for 72 hours in 6-well plates in 5% CO_2 at 37 °C. After the THP-1 cells were differentiated into adherent M0 macrophages, cells were rested for 2-24 hours in PMA-free complete RPMI media before polarization into M1- and M2-like macrophages.

Polarization of M0 macrophages into M1- and M2-like macrophages

M0 macrophages were polarized into M1 macrophages by the addition of 1 ng/mL lipopolysaccharides (# L4391; Sigma-Aldrich, St. Louis, MO) and 20 ng/mL interferon gamma (IFNγ) for 48 hours. M2a macrophages were obtained by incubation in 50 ng/mL human IL-4

recombinant protein (PeproTech-200-04-20ug) in complete RPMI for 48 hours. M2c macrophages were obtained by treatment with 50 ng/mL human IL-10 recombinant protein (PeproTech 200-10-10UG) in complete RPMI for 48 hours. Each molecular/cytokine-containing medium was refreshed every day. Upon 72-hour differentiation, 2- to 24-hour resting, and 48-hour polarization, macrophages in each phenotype were acquired from the 6-well plate with AccutaseTM cell dissociation reagent (Gibco, Waltham, MA) using a cell scraper. Detached cells were centrifuged at 270 g for 8 minutes, and the pellet was reconstituted with 50:50 serum-free media for mixing with fibroblasts.

3D ring tissue fabrication

Rings of fibroblast-only and macrophage-fibroblast mixtures were fabricated in non-adhesive scaffold-free agarose hydrogel molds with a total of 300,000 cells / 75 μL. For ratio-dependent ring fabrication, M0 macrophages and fibroblasts were prepared in 50:50 in ratios of 2:1, 1:4, 1:8, 1:16, and 1:32. After thorough mixing, 75 μL of each mixture was pipetted into the pre-media-equilibriated agarose hydrogel mold in each well of a 24-well plate. Rings were fed with an additional 1 mL of 50:50 media very slowly using a portable Drummond Pipet-Aid. (4-000-100; Drummond Scientific Company, Broomall, PA) 1 hour after seeding. Plates were incubated in 10% CO_2 37 °C incubator and refreshed with 50:50 media the next day, and repeated feeding every other day. For media optimization, 0.1% FBS, 1% FBS, and 10% FBS were added to 50:50, and complete DMEM and complete RPMI were used to make a concentrated cell suspension of each cell type to fabricate the co-culture rings in each medium. Rings were repeatedly fed with the corresponding medium until the end time point. For the fabrication of M1-like or M2-like macrophages to a fibroblast or myofibroblast co-cultured ring, a 1:16 ratio of macrophages to fibroblast cocktail was prepared in a 50:50 ratio.

Tissue thickness measurement and statistical analysis

Brightfield microscopy images on rings of their *x, y*-, and *z*-dimension were acquired using Nikon Eclipse Ts2 microscope (Nikon, Tokyo, Japan) at 2x magnification. On day 7, gels with 3D ring tissues were taken out of the wells and chopped with a razor blade using a 3D printed custom chopping block to trim the cylinder-shaped gel into a cuboidal shape, allowing visualization of the *z*-dimension of the ring by laying the gel on its sides.

The Nikon Eclipse Ts2 microscope was used to obtain images of the rings and *x, y*-thickness measurements were made using NIS Elements AR software (version 6.10.01; Nikon, Tokyo, Japan) (Figure 2A). *Z*-dimension images were obtained using the Nikon Eclipse Ts2 at 2X magnification for all four sides of the cuboidal-shaped gel. The *z*-thickness was measured manually using NIS Elements D (version 6.02.03) for five measurements from each plane on four planes, making a total of 20 measurements per ring (Figure 2B). The Excel file acquired from both *x, y*- and *z*-thickness measurements was then statistically analyzed using Prism (GraphPad Prism version 11.0.0 for Windows, GraphPad Software, Boston, Massachusetts USA, www.graphpad.com). Statistical significance was determined by either ordinary one-way ANOVA or two-way ANOVA. All quantitative data were graphed in box plots with mean ± standard deviation. Statistical significance ($p<0.05$) is visually presented with the asterisk symbol. * denoted $p<0.05$, ** denoted $p<0.005$, *** denoted $p<0.001$, and **** denoted $p<0.0001$.

Macrophages and fibroblast localization in 3D ring tissue

THP-1 derived M0 macrophages and jNHDF cells were prelabeled with CellTracker dyes to fabricate a 1:8 mixture of macrophages to fibroblast co-culture rings. For a total of 300,000 cells

per ring, 17,647 M0 macrophages were stained with 15 uM CellTracker Violet, and 2,823 fibroblasts were stained with 15 μM CellTracker Red. The majority of remaining fibroblasts were not labeled. Rings were acquired at the desired time point and fixed overnight in formalin at 4 °C in the gel. Formalin-fixed tissues were carefully removed from the gel and washed in PBS three times, and kept in PBS in a 96-well plate. SCALEVIEWS4 tissue clearing solution was prepared in advance with published guidelines (Hama et al., 2015) by combining 20 g D(-)-sorbitol, 5 mL glycerol, 12 g urea, 100 μL Triton X-100, 7.5 mL DMSO with deionized water. The total volume of the solution was brought to 50 mL with deionized water. To dissolve all the components, the mixture was heated in a 37 °C water bath and stored in 4°C. 5 minutes before imaging using PerkinElmer Opera Phenix Plus Screening High-Content Screening System (Waltham, MA), tissues were treated with SCALEVIEWS4 solution for 1-2 minutes until transparent, washed with PBS, and placed on a drop of SCALEVIEWS4 solution on the bottom of a 24-well black plate with a glass bottom (Cellvis, Mountain View, CA). The images were acquired using a 5x air objective and a 20x water-immersion objective.

Cell viability in 1:16 macrophages to fibroblast ring

Before seeding, all 17,647 M0 macrophages were labeled with CellTracker Violet (15 μM) and 17,647 fibroblast cells were labeled with CellTracker Red (15 μM) in PBS at 37 °C and 10% CO_2 on a shaker for 30 minutes. CellTracker-labeled cells were rinsed thoroughly with PBS before being mixed with the additional 264,706 unlabeled fibroblasts in a 1:16 co-culture mixture. 75 μL volume of the final mixture was seeded to fabricate a 3D ring tissue. On days 2 and 7, a ring from each group was collected and liberated into single cells. Rings were treated with 2.5 mg/mL collagenase A (Roche, Basel, Switzerland) and 1 U/mL dispase II (Sigma-Aldrich, St. Louis, MO) for 60-90 minutes at 37 °C in 10% CO_2, with periodic pipetting.

Dissociated cells were thoroughly rinsed with 0.5% BSA PBS, and centrifuged cell pellets were resuspended in 1 mL of 0.5% BSA PBS and seeded back to poly-D-lysin pre-treated glass-bottom 12-well black plate (Cellvis, Mountain View, CA). The plate was stored at 37 °C for 2 hours. Cells not adherent were aspirated and an additional 1mL of PBS was added before being visualized under fluorescent ZEISS Axio Observer.Z1. Each CellTracker-labeled adherent cell was counted from 5% of the region of interest (ROI) using FIJI (Fiji is Just ImageJ) software in 4 replicates. Quantitative data on the ratio of counted macrophages to fibroblasts were visualized and statistically analyzed using Prism. The statistical significance of quantified cell count from each 4 ROI was determined by ordinary two-way ANOVA. All the quantitative data were visualized in bar graphs with ± standard deviation, and each dot represents cell counts from an ROI.

Collagen synthesis measurements and quantification

To measure collagen synthesis, an ELISA for the Procollagen Type 1 C-Peptide (PIP) (Takara, Shiga, Japan) was used. Supernatants were collected on day 2, 4, and 7, and levels of P1CP measured. Detection of soluble Procollagen I C-terminus propeptide (P1CP) levels in the supernatant stoichiometrically reflects collagen I synthesis. After fresh media were added following supernatant collection, the media were completely aspirated after 15 minutes to remove any remaining P1CP. Then, fresh media were added and incubated at 37 °C and 10% CO_2 until the following sample collection. Biological triplicates were analyzed by collecting their supernatants, centrifuging at 1000 rpm for 5 minutes, transferring the supernatants to new microcentrifuge tubes, and storing them at -20 °C upon use.

Samples were thawed at room temperature, and 10 µL were diluted with 40 µL of sample diluent (1:5 dilution) from the kit. (Takara, Shiga, Japan) The assay was performed according to

the manufacturer's protocol. Additionally, phosphate-buffered saline (PBS) 1X was used as a washing buffer, and 1N hydrochloric acid (HCl) was used as a stop solution. Serial standard dilutions were performed over a range of 640 ng/mL to 10 ng/mL in uncoated 96-well plates. After the stop solution was added and mixed, 180 µL samples were transferred into a new 96-well plate to measure absorbance at 450 nm using a plate reader (Varioskan Lux, Thermo Scientific, Waltham, MA). 4-Parameter Logistic (4-PL), a sigmoidal nonlinear regression model, was used to fit the standard curve and further analyze the quantified absorbances using the ELISA Data Analysis tool provided by Boster Bio (Boster Bio, Pleasanton, CA). The results were visualized and statistically analyzed using GraphPad Prism 10.

Immunohistochemistry/Immunocytochemistry markers

A mouse anti-human CD68 monoclonal unconjugated antibody (50-112-2650; InvitrogenTM, Carlsbad, CA) was used as the primary pan-macrophage marker at a 1:500 dilution for IHC and at a 1:100 for ICC. The mouse anti-human CD86 monoclonal unconjugated antibody was reconstituted to 0.5 mg/mL in sterile PBS. Mouse anti-human CD86 (MAB108521SP; R&D Systems, Minneapolis, MN) was used as the primary antibody for M1 macrophages at a 1:100 dilution. Rabbit anti-human CD206 (Human Mannose Receptor) monoclonal unconjugated antibody was used as an M2a macrophage marker (ZRB1440-25UL; Sigma-Aldrich, St. Louis, MO). Lyophilized CD206 antibody was reconstituted with sterile PBS at 1 mg/mL and diluted to 1:100. Rabbit anti-human CD163 polyclonal unconjugated antibody (NBP2-48846-25ul; NOVUS biologicals, Centennial, CO) was used as a M2c macrophage marker at 1:2500 dilution. Rabbit anti-human alpha-Smooth Muscle Actin (αSMA) (ab5694; Abcam, Cambridge, UK) polyclonal unconjugated antibody was used as a myofibroblast marker at a 1:200 dilution. Goat anti-rabbit IgG H&L Alexa Fluor 568 was used as a secondary antibody (2 µg/mL). Goat

anti-mouse IgG (H+L) Alexa Fluor 647 (Invitrogen, Carlsbad, CA) was used as a secondary antibody (2 μg/mL).

Immunostaining

To visualize macrophage and fibroblast differentiation, repolarization (shift between phenotypes), or depolarization, immunophenotyping was performed using fluorescent immunohistochemistry. Rings in the gel collected on day 1, 2, 4, and 7 were fixed with 10% formalin for 4 hours. Ring tissues removed from the gel were transferred to 15% w/v sucrose, followed by 30% w/v sucrose. Sunken ring tissues were embedded in O.C.T compound (Sakura Finetek, Torrance, CA; Fisher Scientific, Waltham, MA) on a cryomold (Sakura Finetek) either vertically or horizontally, frozen on dry ice, and stored at -80 °C until sectioning. Cryosections were performed with a QS12 cryostat (Avantik, Pine Brook, NJ) on positively charged microscope slides (Fisher Scientific, Waltham, MA). For stable adhesion, slides were baked in a 65 °C oven for 3-5 minutes and stored at -80 °C until usage.

Slides were baked in 65 °C oven for 3 minutes, immersed in PBS to dissolve the O.C.T compound, heat induced epitope retrieval (HIER) was done with tris-EDTA pH 9.0 for 35 minutes, blocked with 10% normal goat serum (NGS), 1% bovine serum albumin (BSA), and 0.1% Triton X-100 for 1 hour at room temperature, and labeled with primary antibody for overnight at 4 °C. To visualize the primary antibody, either anti-mouse or anti-rabbit IgG antibody was incubated for 30 minutes at room temperature, followed by counterstaining of nuclei with DAPI (Invitrogen, Carlsbad, CA) for 2 minutes. The tissue was covered with ProLong Diamond Antifade mountant (Invitrogen, Carlsbad, CA) and coverslipped. Slides were stored in 4 °C until imaged under Evident Olympus VS200 Slide Scanner (Olympus, Tokyo, Japan) at 20X magnification. Images were analyzed using open-source software, QuPath.[19]

To confirm the macrophage phenotypes, cells were stained in 2D. PMA-treated THP-1 cells were cultured on the coverslips treated with poly-D-lysine in a 12-well plate. Post 72 hours differentiation, 24 hours of resting, and 48 hours of polarization, macrophages were fixed with 4% paraformaldehyde (PFA) for 10 minutes. Fixed samples were permeabilized with 0.1% Triton-X 100, blocked with 10% NGS and 1% BSA in PBS, labeled with primary antibody overnight at 4 °C, incubated with secondary antibody at room temperature for 30 minutes, and counterstained with DAPI for 2 minutes. The coverslip was lifted from the well and mounted onto slides with Prolong Antifade Mountant (Invitrogen). The slides were stored at 4 °C and imaged with a VS200 slide scanner at 40X magnification. Images were analyzed using open-source software, QuPath.

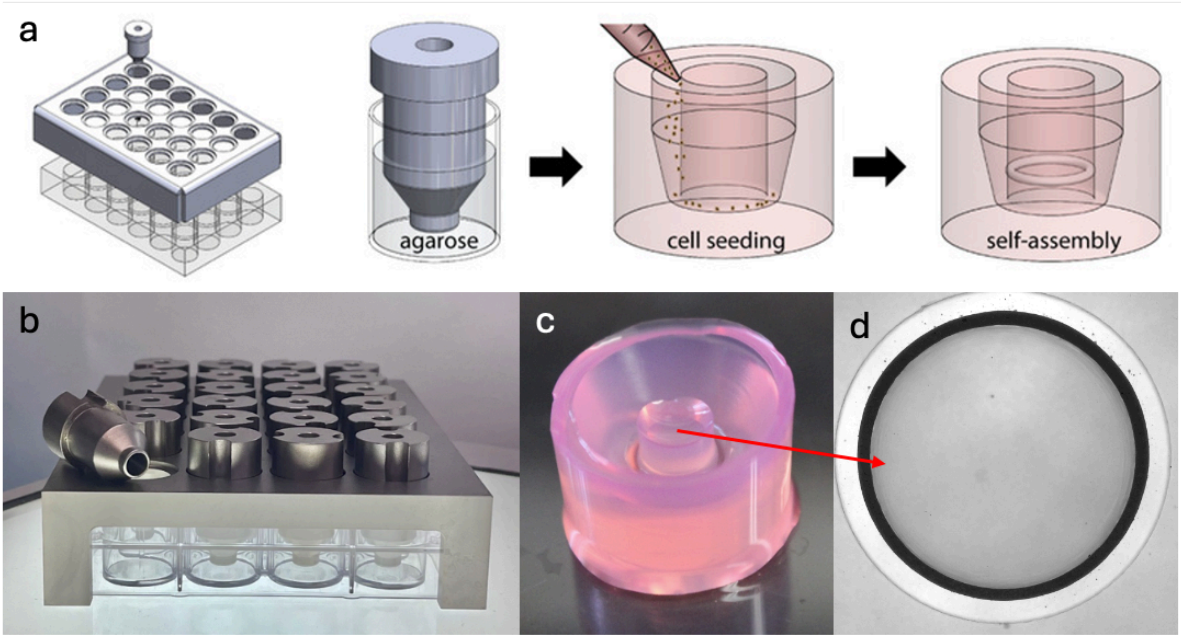

Figure 1. Fabrication of 2% w/v agarose mold to produce 3D ring-shaped tissues. (a) Schematic illustration of the mold fabrication process and cell seeding procedure used to generate the 3D ring tissue structure.[20] (b) Photograph of the 25-piece stainless steel mold positioned on a 24-well plate. (c) Representative image of the media-equilibrated 2% w/v agarose mold. (d) Representative top-down *x, y*- dimension image of the day 2 ring acquired under bright-field microscopy at 2x magnification.

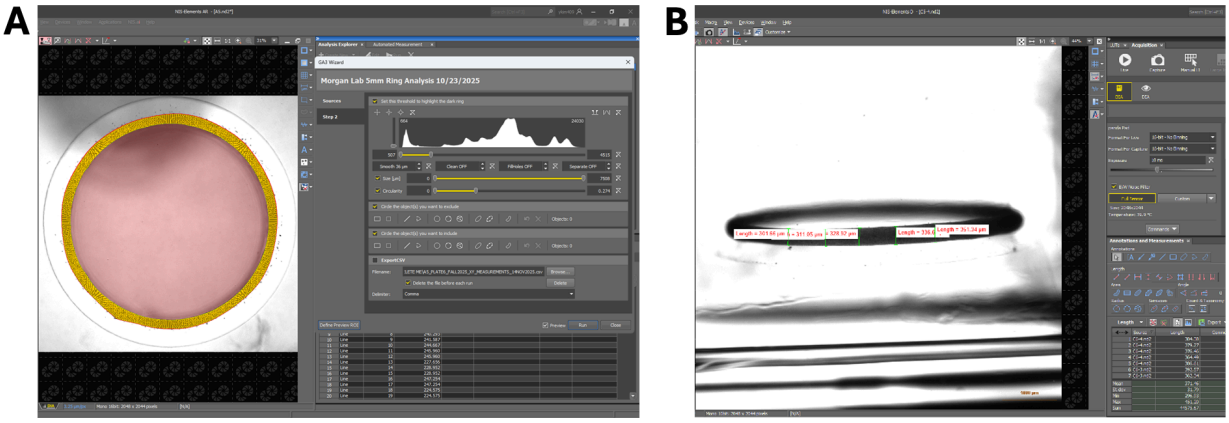

Figure 2. *x, y*-, and *z*-dimension ring thickness measurement using NIS-Elements software. (A) Representative image of ring thickness analysis performed using NIS-Elements AR software with automated measurement code to obtain thousands of thickness measurements across the ring perimeter. (B) Representative image of *z*-dimension thickness measurement performed using NIS-Elements D software. For *z*-thickness analysis, measurements were manually taken at five locations on each of the four sides of cuboidal gel samples placed on their sides, yielding a total of 20 z-thickness measurements per sample.

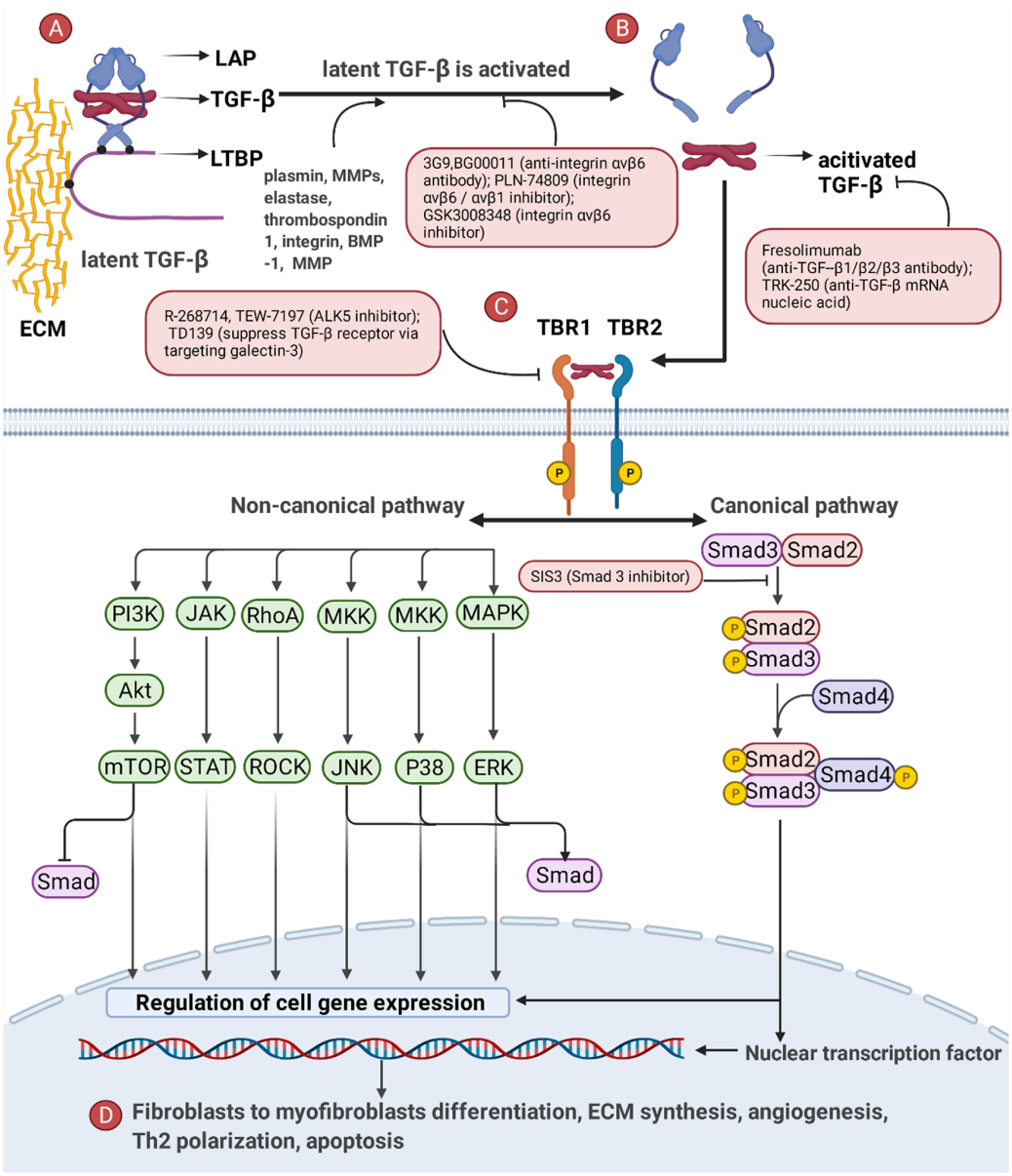

Figure 3. Fibrogenesis signaling cascade activated by TGF-β. The critical role of the TGF-β pathway and drugs targeting the TGF-β pathway in idiopathic pulmonary fibrosis with corresponding preclinical drug candidates. (A) Latent TGF-β (TGF-β trapped in LAP) binds to ECM through LTBP. (B) TGF-β is detached from LAP and activated only in the presence of specific stimuli. (C) Activated TGF-β activates the downstream SMAD-dependent pathway (canonical pathway) and SMAD-independent pathway (non-canonical pathway). (D) The TGF-β pathway, activated by fibroblasts and immune cells, influences fibroblast-to-myofibroblast differentiation, ECM synthesis, angiogenesis, Th2 polarization, and apoptosis (Figure from Ma H. et al. 2022).[15]

Results

3D Ring formulation and effect of serum on ring-structure stability

Adopted from Tan et al's 3D spheroid hybrid culture study, a 1:16 ratio of macrophages to fibroblasts was cultured in multiple media conditions to see the effect of serum concentration.[16] Previous work demonstrated the impact of serum on 3D ring tissue formation and showed that serum disrupted the structural integrity of ring-shaped tissues, leading to loss of uniformity over time.[20] Consistent with these findings, rings cultured in complete RPMI and in 50:50 supplemented with 10% FBS showed progressive thinning over later time points (Figure 4). In contrast, rings cultured in serum-free media or at lower serum concentrations maintained consistent morphology and structural integrity across all time points. Serum-dependent ring-structure retention was tested with 8 rings per condition. 1% FBS 50:50 retention was the lowest, with 50% maintenance in ring-structure by day 7. At the same time, the 50:50 and complete RPMI yielded 75%, and others yielded above 87.5% (Figure 6A).

Localization of M0 macrophages and fibroblasts in the ring tissue

To determine whether different media conditions affected cell distribution within the 3D ring tissues, confocal imaging was performed to visualize the localization of two different cell types labeled with CellTracker. 1:8 of M0 macrophage to fibroblast ring tissue, 17,647 M0 macrophages (50% of macrophage population) were labeled with CellTracker violet (15 μM), and 2,823 fibroblasts (1% of fibroblast population) were labeled with CellTracker red (15 μM). Across all media conditions, both cell types were uniformly distributed throughout the ring structure on day 1 rings. Whole-ring projections at 5x, single *z*-stack images taken at the core of the tissue at 20x, and combined projections of *z*-stacks at 20x (Figure 5, top row to bottom,

respectively) demonstrate a homogeneous distribution of each cell type across each culture medium. These results suggest that media composition does not significantly impact the initial spatial organization of co-cultured cells within the 3D ring structure, indicating that the fabrication method reliably supports homogeneous cell incorporation.

Ring Structure Stability

Structural stability of the 3D ring shape was assessed by monitoring ring integrity over time across different media conditions to optimize media conditions. Rings cultured in high-serum-containing media exhibited structural disruption, as shown in Figure 4. The addition of 1% FBS to 50:50 media resulted in the lowest structural integrity until day 7, with a yield of 50% maintaining ring-shaped structure without breakage. In comparison, 0.1% FBS addition to 50:50 resulted in 100% structural retention until the endpoint (Figure 6A). 50:50 serum-free and complete RPMI yielded 75%, while 10% FBS 50:50 yielded 87.5%. Thinning of the tissue morphology cultured in a higher FBS concentration caused ring breakage when the rings were lifted from the gel peg for further analysis of cell viability. Ring breakage may be attributed to hydrogel variability; the overall trend consistently demonstrates improved stability under low-serum or serum-free conditions.

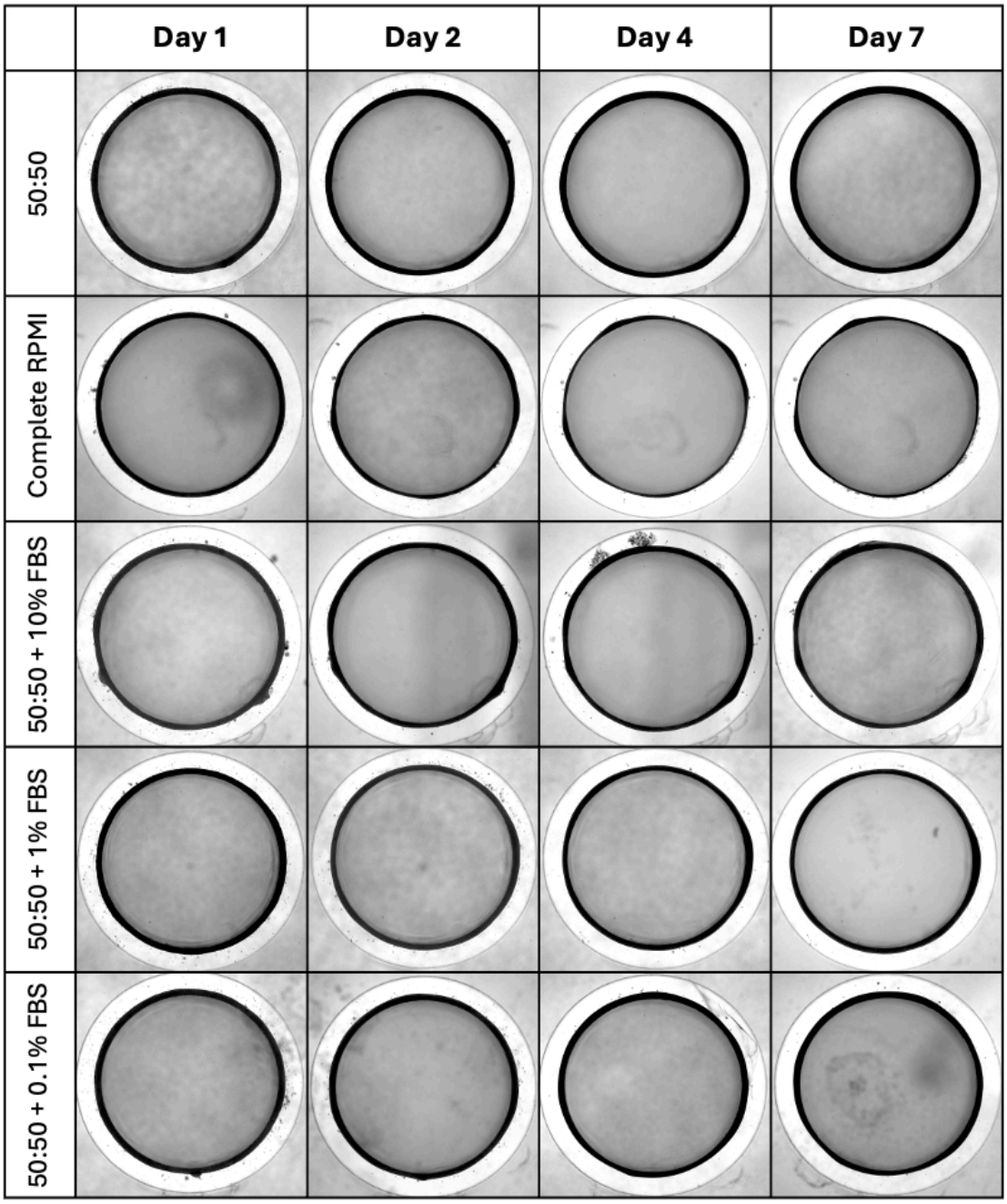

Figure 4. Bottom-view bright-field images of 3D ring tissues on days 1, 2, 4, and 7, from left to right. The columns indicate culture time, and the rows indicate culture conditions: 50:50, complete RPMI, 50:50 + 10% FBS, 50:50 + 1% FBS, and 50:50 + 0.1% FBS. The gray circular region surrounding the 5 mm agarose peg indicates the tissue area used for *x*- and *y*-dimension analysis.

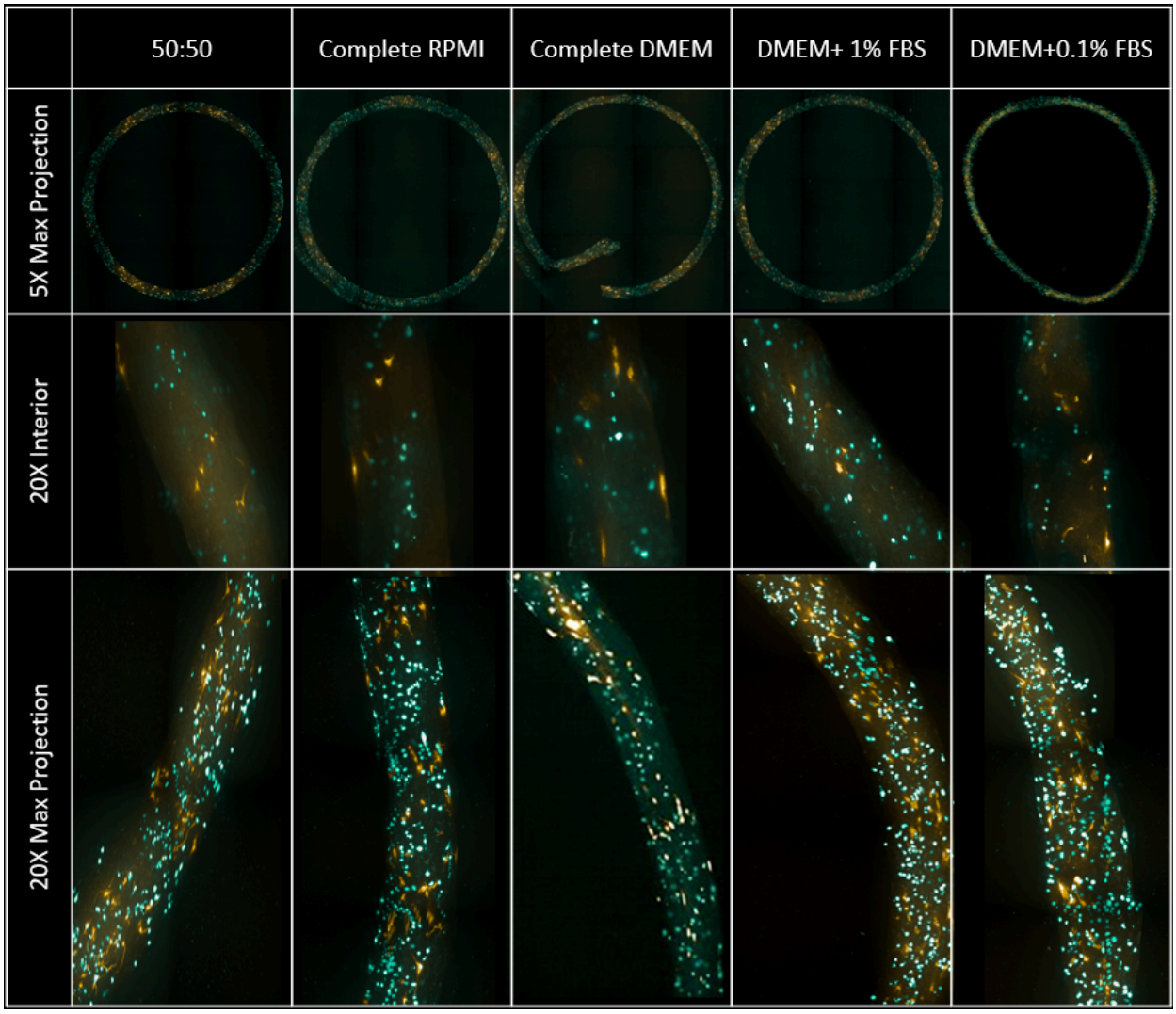

Figure 5. Confocal images of 3D ring tissues on day 1 cultured in different media. 2,823 fibroblasts and 17,647 M0 macrophages were labeled with CellTracker Red and CellTracker Violet, respectively, to visualize cell localization within the 1:8 macrophage-to-fibroblast ring. Equivalent numbers of labeled cells were seeded in each condition. The top row shows 5x maximum projection images. The middle row shows 20x single-confocal *z*-stack images of the ring core. The bottom row shows 20x maximum projection images. All rings were collected on day 1 post-seeding, fixed in formalin, and cleared using the ScaleS4 solution.

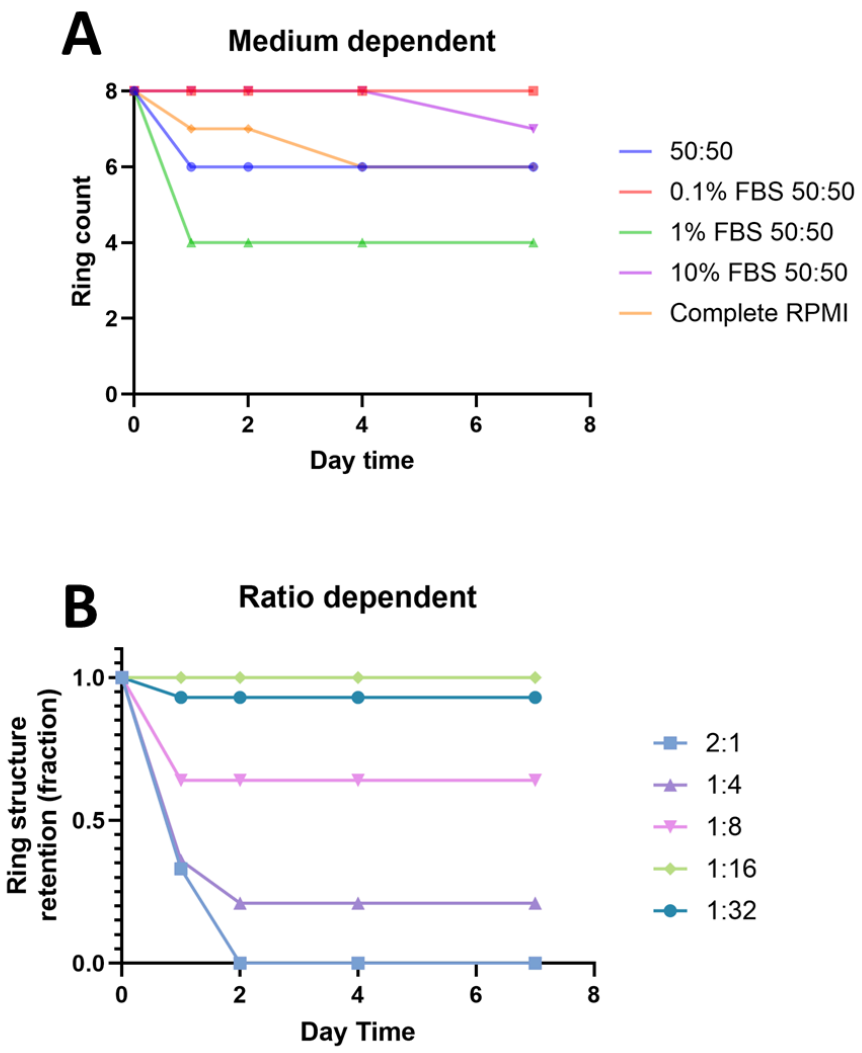

Figure 6. Quantification of ring structure as a function of culture medium and macrophage-to-fibroblast ratio. (A) Rings were cultured at a macrophage-to-fibroblast ratio of 1:16 in different culture media. The percentage of rings that maintained their structure through day 7 was determined. A total of 8 rings were seeded for each condition.
(B) Rings were cultured with macrophage-to-fibroblast ratios of 2:1, 1:4, 1:8, 1:16, and 1:32, and the percentage of rings that maintained their structure through day 7 was determined. A total of 14 rings were seeded for 1:4, 1:8, 1:16, and 1:32 conditions. A total of 3 rings were seeded for the 2:1 condition.

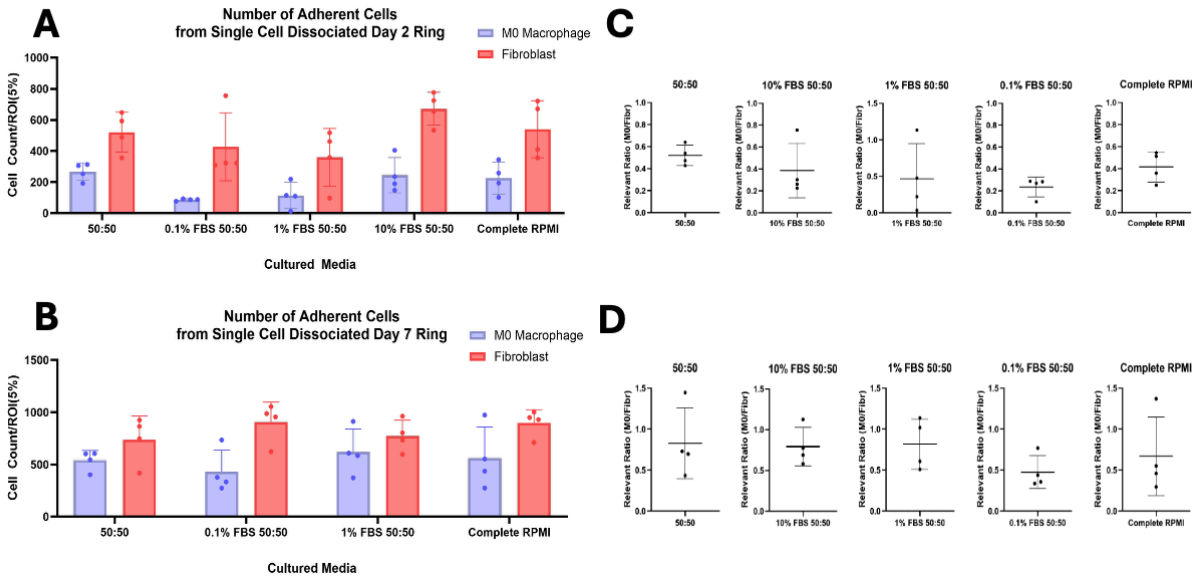

Figure 7. Cell viability assay for media optimization.
17,647 cells of M0 macrophages and fibroblasts were labeled with CellTracker dye violet and red, respectively, and seeded to fabricate a self-assembled 1:16 macrophage to fibroblast ring tissue. On days 2 and 7, rings were acquired, liberated into single cells, and plated onto a 12-well black-wall glass plate. Adherent cells were visualized under fluorescent microscopy. **(A-B)** The number of cells in each well was counted under a fluorescent microscope and analyzed with FIJI using a region of interest (ROI) at 5%. Each dot represents an analysis from 1 ROI. (A) number of adherent cells of each cell type in a different culture medium from day 2 ring, n=1. **(B)** number of adherent cells of each cell type cultured in a different medium from day 7 ring, n=1. **(C-D)** Ratio of counted macrophages to fibroblasts to see the comparison of the viability of each cell cultured in different media from day 2 on top and day 7 on the bottom.

50:50 and 0.1% 50:50 showed the most viable cells until day 7

To evaluate cell survival within the 3D ring tissues and to select optimal culture medium, a total of 17,647 M0 macrophages and 17,647 fibroblasts were pre-labeled with CellTracker violet (15 μM) and red (15μM). Quantification of adherent CellTracker-pre-labeled macrophages and fibroblasts following tissue dissociation at defined time points was used to evaluate cell viability and proliferation. On day 2, rings cultured in serum-free 50:50 media exhibited the highest number of viable macrophages, indicating that serum-free conditions did not cause serum

deprivation or cell death in early macrophages. (Figure 7A) By day 7, 1% FBS 50:50 showed the highest macrophage counts, followed by serum-free 50:50 and complete RPMI (Figure 7B). In contrast, fibroblasts demonstrated increased cell numbers in serum-containing conditions at later time points, suggesting proliferation in 50:50 or complete RPMI media supplemented with serum. To analyze the relative population of non-proliferating THP-1-derived macrophages and a possible proliferating fibroblast, the relative numbers of each cell were expressed as percentiles. Serum-free 50:50 maintained the highest relative macrophage to fibroblast across conditions on both day 2 and day 7 (Figure 7C and 7D). These findings suggest that while low levels of serum slightly enhance long-term macrophage viability, serum-free 50:50 provides a more balanced and controlled environment for maintaining both cell populations without excessive fibroblast proliferation. Notably, 1% FBS 50:50 showed intermediate cell viability and structural uniformity but poor preservation of ring structure. Taken together, these results identify serum-free 50:50 as the optimal culture medium that supports structural integrity, balanced cell viability, and reproducibility of the 3D ring model. Hereafter, a macrophage and fibroblast co-culture was performed in 50:50 serum-free media.

Ratio of macrophages to fibroblasts for co-culture

To determine the optimal macrophage-to-fibroblast ratio for stable 3D ring formation, co-culture conditions were evaluated across 2:1, 1:4, 1:8, 1:16, and 1:32 ratios in serum-free 50:50 media (Figure 6B). These ratios were selected to capture both macrophage-dominant and fibroblast-dominant conditions and to approximate physiologically relevant cellular compositions during fibrogenesis. Rings formed under extreme ratios, particularly macrophage-dominant conditions, in 2:1, observed reduced preserved structural integrity and inconsistent tissue formation from day 1. In contrast, fibroblast-dominant conditions supported

better preservation of the ring structure. Among the tested conditions, the 1:16 macrophage-to-fibroblast ratio consistently produced stable, uniform ring structures with 100% stability throughout the study. A preliminary study by Tan et al. demonstrated that the 1:16 ratio mimics the most physiologically relevant microenvironment in tissue fibrogenesis [16]. The 1:16 ratio, therefore, represents the most balanced structural stability and biological relevance to be analyzed and is selected as the optimal co-culture condition for all subsequent experiments in this research.

Phenotypic characterization of macrophages

To evaluate macrophage phenotype and their influence on fibroblast activation within the 3D ring model, immunofluorescence staining was performed using macrophage markers. CD68, a pan-macrophage marker, was detected in all co-cultured rings (M1, M2a, and M2c). For M1, the CD86 primary antibody was visualized. M2a and M2c were visualized with CD206 and CD163, respectively. CD86 was slightly visible at the edges at the 1:50 dilution, and will be further optimized with this dilution. CD206 and CD163 were visualized at working concentrations of 1:100 and 1:2500, respectively (Figure 8), but were not detected in time-dependent cryosections (Figure 9). A positive CD68 signal in M1, M2a, and M2c co-cultured rings indicates that macrophages are present, but the polarization marker needs to be further optimized (Figure 9).

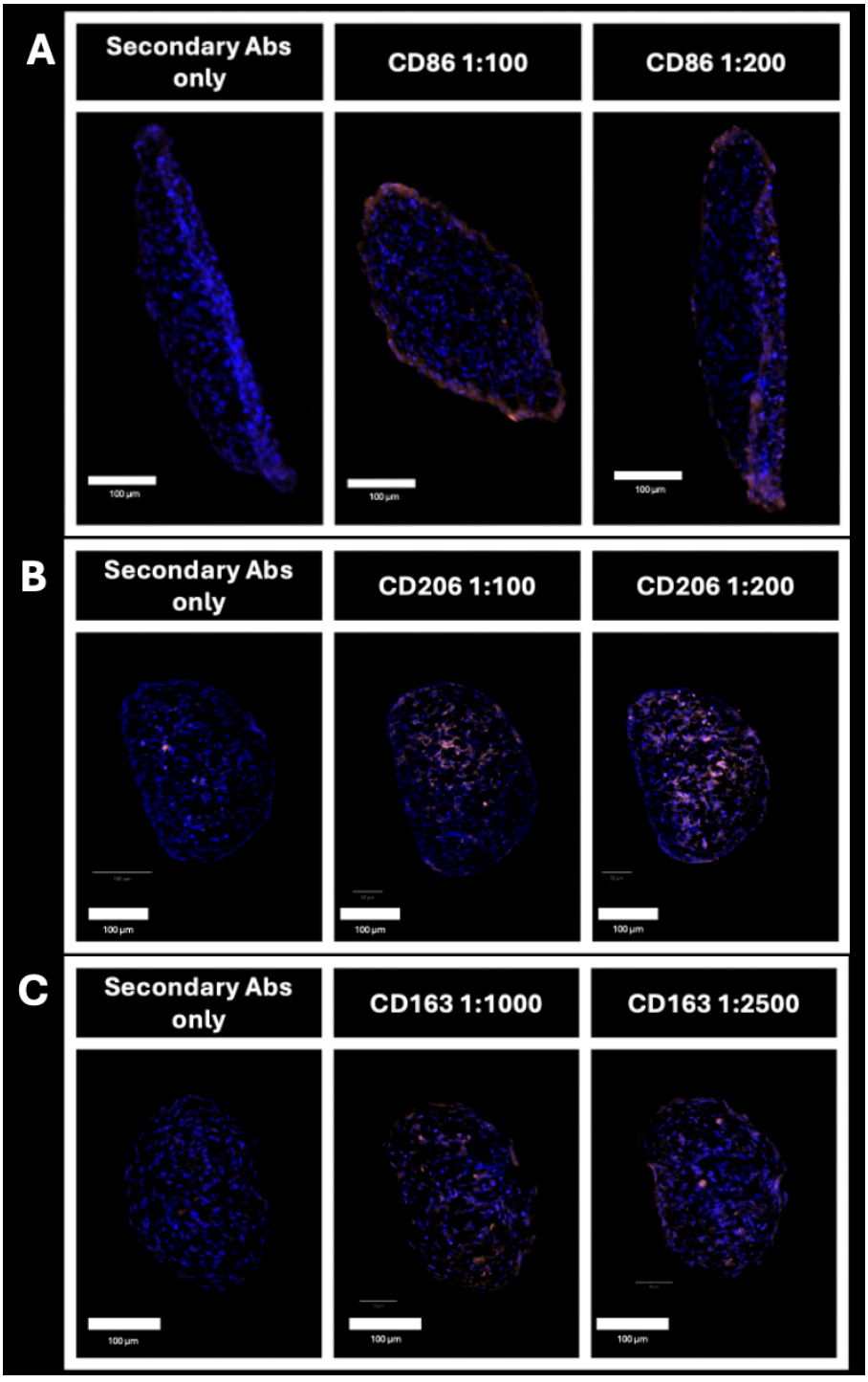

Figure 8. Primary antibody titration for CD86, CD206, and CD163 as markers for M1, M2a, and M2c, respectively, with a negative control. CD86, CD206, and CD163 primary antibodies were titrated according to the vendor's recommended working concentrations. The middle column was selected as the final working dilution for each marker compared to the secondary-only negative control. Scale bar = 100 μm.

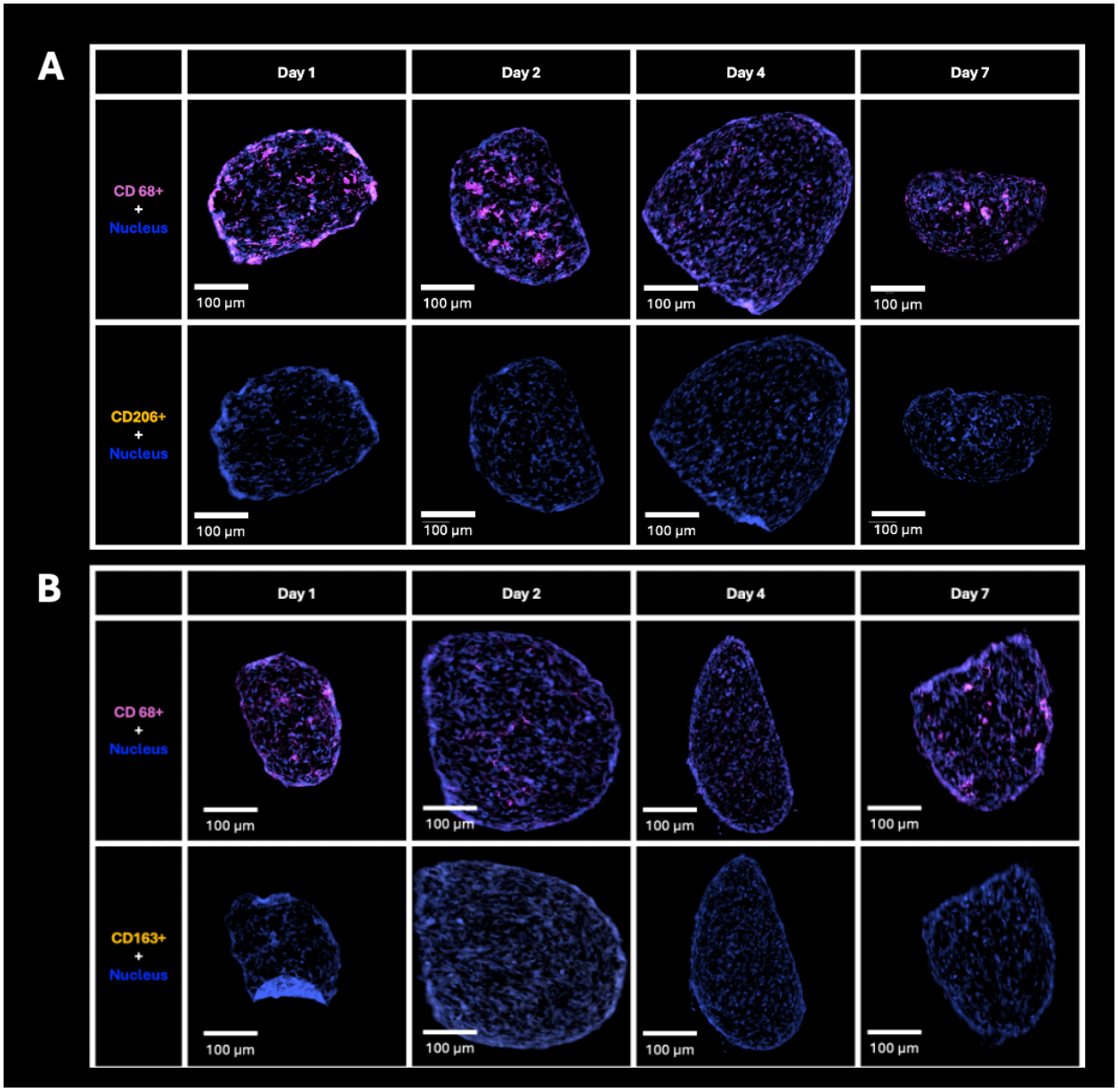

Figure 9. Pan-macrophage marker with M2a and M2c markers
(A) M2a-CD206 primary and secondary antibody staining on M2a co-cultured rings on each day, with nuclei counterstaining with DAPI on serial sections. (B) M2c, CD163, primary and secondary antibody staining on M2c co-cultured rings on each day, with nuclei counterstaining with DAPI on serial sections. Scale bar = 100 µm.

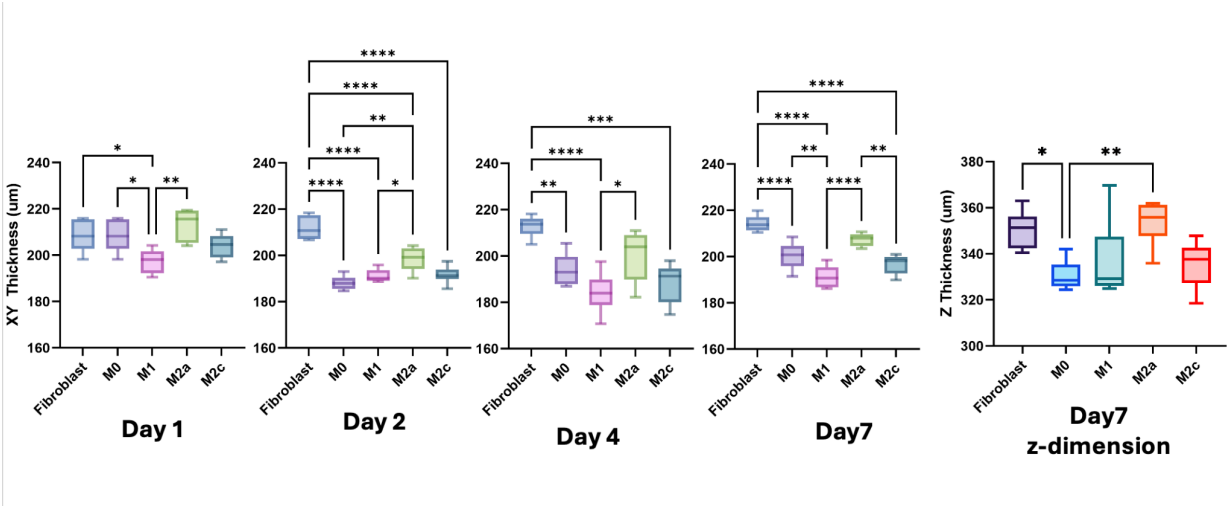

Figure 10. *x, y*- and *z*-thickness measurements and statistical analysis on each macrophage phenotype-fibroblast 1:16 co-culture ring. Six rings per group were taken under 5x brightfield, and thousands of *x, y*-thickness measurements were quantified for each ring over time until day 7. *z*-dimensional thickness was quantified for 20 spots for each ring and averaged. Statistical significance ($p<0.05$) is visually presented with the asterisk symbol. * denoted $p<0.05$, ** denoted $p<0.005$, *** denoted $p<0.001$, and **** denoted $p<0.0001$.

Structural characterization of 3D ring tissues

To evaluate how macrophage phenotype alters tissue morphology, *x, y*-, and *z*-dimensional thickness measurements were compared across co-culture conditions (Figure 10). In fibroblast and macrophage co-culture rings, M1 co-culture consistently exhibited lower *x, y*-thickness than the fibroblast-only control across all time points. In contrast, the other macrophage co-culture conditions were initially comparable to fibroblast-only rings on day 1, at around 200-220 µm, but significantly declined in thickness from day 2 onward, to around 180-210 µm. Among these groups, M2c showed thickness values most similar to the M0 co-culture condition. Interestingly, day 7 *z*-dimension analysis showed that the M2a co-culture condition produced a similar thickness to fibroblast-only rings, suggesting that *x, y*- and *z*-dimensional tissue organization may not change in parallel. Because tissue thickness in this

system is influenced by multiple structural features, including contractility, extracellular matrix organization, and cell alignment, these measurements should be interpreted as a composite structural readout rather than a direct indicator of fibrotic activity. Additional analysis of day 7 cross-sectional area may further clarify how tissue geometry differs across macrophage phenotypes.

In myofibroblast co-culture rings, the trend of tissue thickness compared between macrophage phenotypes was distinct from fibroblast-macrophage co-cultured rings (Figure S2). Visual inspection in Figure S3 showed that these tissues were less uniform and often appeared puffier or rougher, which likely contributed to the larger variability observed in quantitative measurements. Despite this variability, all macrophage co-culture conditions were, on average, slightly thicker on a co-cultured ring than that of the myofibroblast-only control. The average thickness was around 250 μm on day 1 and showed slight contraction below 250 μm from day 2, with slight expansion until day 7. Unlike fibroblast co-cultured settings, M2-associated conditions in myofibroblasts tended to be slightly thinner, although the differences were modest overall. Additionally, in contrast to fibroblast co-culture settings, the M0 basal macrophage condition tended to remain thicker until day 7. Together, these findings suggest that the M1 and M2 macrophage phenotypes play different regulatory roles in tissue compaction in fibroblast co-cultures than in myofibroblast co-cultures.

Collagen production as a functional readout of fibrotic activity

To evaluate the dynamic process of extracellular matrix production within the 3D ring model, collagen type I synthesis was quantified using a Procollagen Type 1 C-terminal propeptide (P1CP) ELISA assay. Supernatants collected from biological triplicates at day 2, 4, and 7 enabled temporal analysis of collagen production across macrophage phenotypes and

co-culture conditions (Figure 11A). In fibroblast co-cultures, profibrotic M2 macrophages exhibited the highest collagen production across time points. The trend of normalized P1CP concentration declined towards later time points except for the M1. Pro-inflammatory M1 macrophages showed lower collagen production than both fibroblast only (-/-) (macrophage negative/polarization negative) and M0 macrophage (+/-) conditions at earlier time points. However, collagen production in M1 co-cultures increased by day 7, and total concentration became similar to that of M2 co-cultured rings.

In myofibroblast co-cultures, the opposite trend was observed compared with fibroblast co-cultures. M2a-like macrophages demonstrated the lowest collagen production across all time. The normalized quantification of P1CP in ng/mL per day showed that the concentration started around 200 ng/mL on day 2, increased to 250 ng/mL on day 4, and dropped to 200 ng/mL by day 7. Compared to the M2a-fibroblast co-cultured ring's P1CP level, which remained above 300 ng/mL at all time points, suggests a switch to a different macrophage-mediated regulatory role in extracellular matrix production, contrasting with the established profibrotic role of M2 macrophages in an already activated myofibroblast environment. In addition, the M1-myofibroblast co-culture showed the highest collagen type 1 production across all time points. Across all myofibroblast-only and macrophage-addition to myofibroblast, there was a slight or moderate decline in total P1CP synthesis towards later time points.

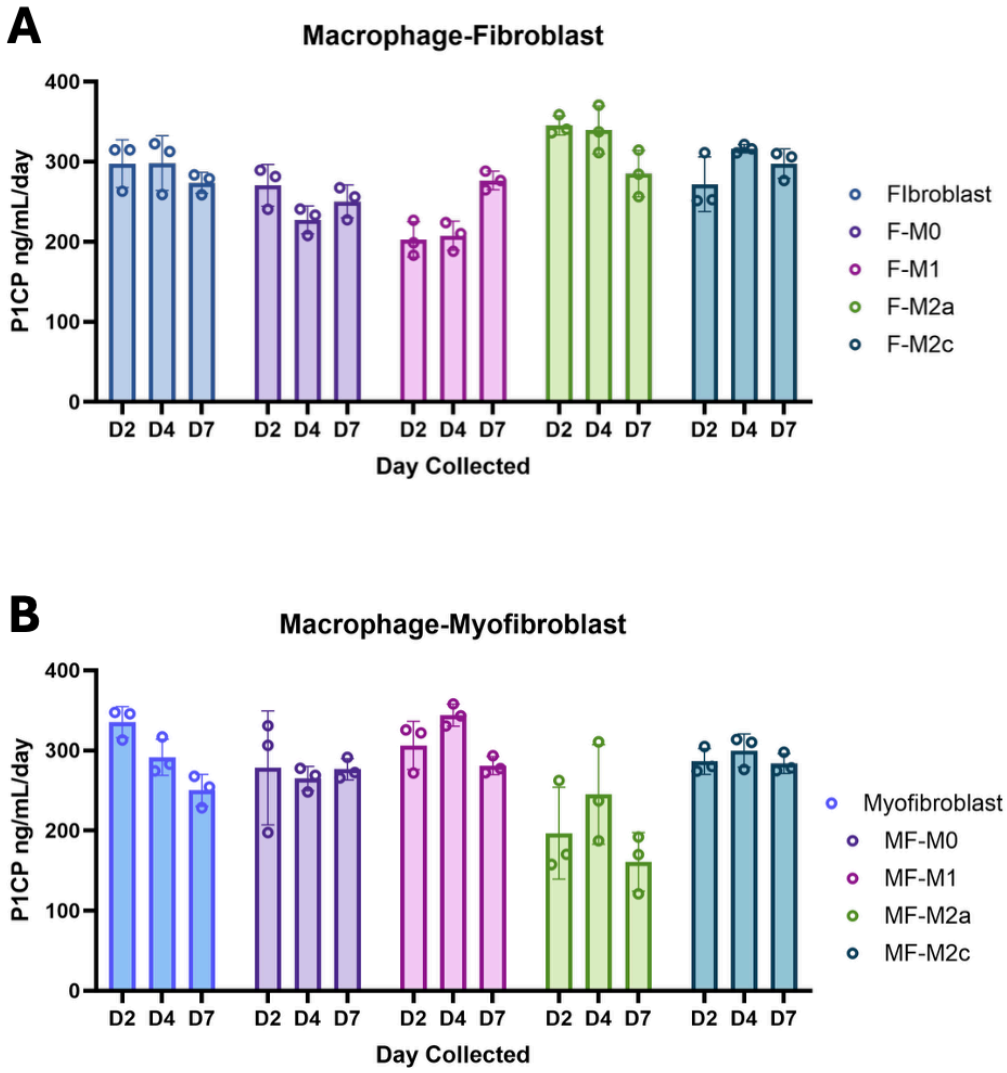

Figure 11. Procollagen type I C-terminus propeptide ELISA analysis of supernatants collected on day 2, 4, and 7.
Periodic collagen production was quantified from supernatants collected on day 2, 4, and 7. (A) P1CP quantified for fibroblast co-culture setting, analyzed that P1CP concentration was higher from day 2 for M2a co-cultured rings, and M2c had a delayed increase in P1CP concentration in the supernatant from day 4. The trend of P1CP decreased over time towards day 7, except for M1 co-cultured rings, which showed an increase towards later time points. (B) In the myofibroblast co-culture setting, the least amount of P1CP was quantified in the M2a-myofibroblast culture, resulting in an opposite outcome to that in the fibroblast co-culture setting. M1 had the highest P1CP on day 4 among all other phenotypes. Except for the M0-myofibroblast co-culture, all other monocultures and co-cultures showed decreased P1CP at later time points.

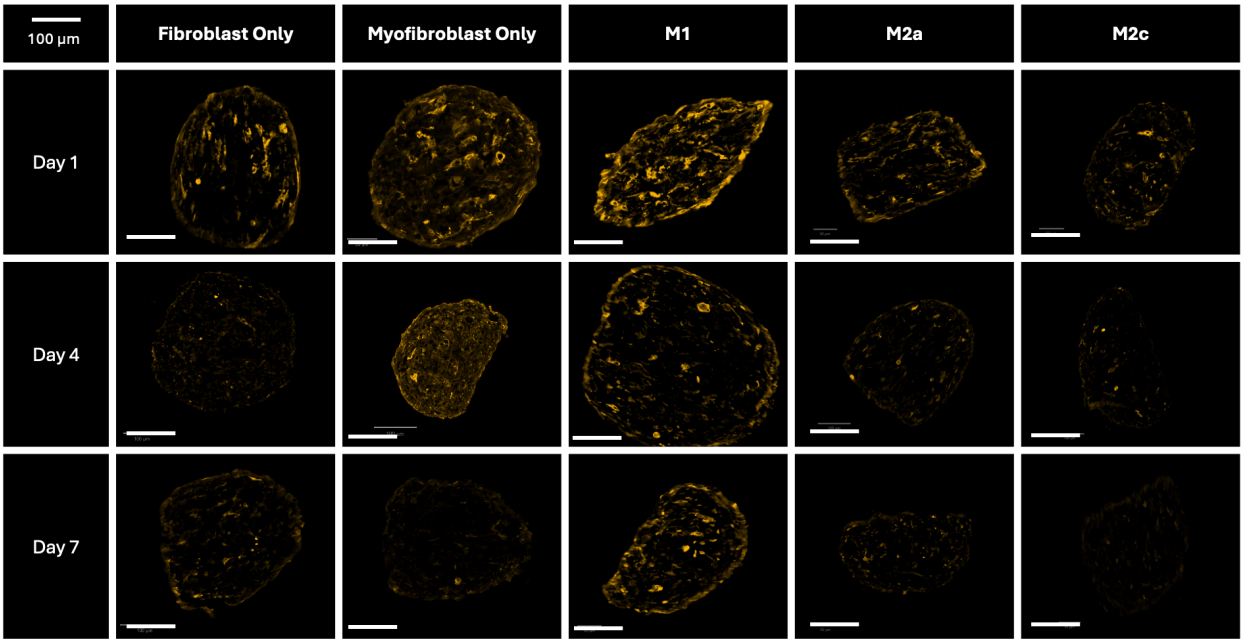

Figure 12. Myofibroblast activation marker, αSMA primary and secondary antibody immunostaining on cross-sectional cryosections of different rings.
The fibroblast-only and myofibroblast-only rings served as negative and positive controls, respectively. M1, M2a, and M2c macrophage co-cultured rings were analyzed for αSMA activation, as shown in the third column from the right. Rows towards the bottom are the progression of co-cultured time. Scale bar = 100 µm.

Myofibroblast activation on macrophage-fibroblast co-culture rings

Along with quantification of collagen production, αSMA activation has been visualized by fluorescent immunohistochemistry. The comparison was made between negative and positive controls: fibroblast-only and myofibroblast-only rings, with M1, M2a, and M2c to fibroblast co-cultured rings (Figure 12). The fibroblast-only ring has the least amount of activated marker of αSMA from day 1. The myofibroblast-only ring showed the most fluorescence as a positive control. M2 co-cultured rings showed higher activation than the negative control (fibroblast only) at the earlier time point. M1 co-cultured rings showed prolonged αSMA expression until day 7 when all other samples showed declining positive signals. This result aligns with the

collagen production level: M1 showed increased synthesis at later time points due to delayed activation of fibroblast-to-myofibroblast transformation (FMT), while the others showed declining collagen accumulation due to dedifferentiation of myofibroblasts.

Discussion

M1 Macrophage Co-culture

M1 macrophage co-culture rings consistently exhibited the lowest *x, y*-thickness across all time points compared to other macrophage phenotypes and the fibroblast-only control. This result might indicate a reduction in ECM production deposited around the tissue structure due to high secretion of matrix metalloproteinases (MMPs), which enhances ECM degradation.[21] The persistent decrease in *x, y*-thickness until day 4 distinguishes M1-mediated morphological formation from that of M2 subtypes, which showed a slight increase in thickness on day 4 compared to day 2. *Z*-dimensional analysis on day 7 further corroborated this pattern, with M1 rings maintaining comparably reduced thickness, suggesting that M1-associated reduced ring volume occurs across all structural axes rather than being limited to the lateral dimension.

The collagen production level in M1 co-cultures demonstrated lower P1CP levels at early time points (day 2 and day 4) relative to both fibroblast-only and M2 co-culture conditions. This consists of the phenotypic role of M1 macrophages that are primarily pro-inflammatory rather than pro-fibrotic. However, a notable increase in collagen synthesis was observed by day 7, at which point P1CP levels reached similar to those of M2 co-cultured rings. This delayed upregulation in collagen production suggests temporal dynamic fibrogenic responses in M1 co-cultures. One possible explanation is macrophage phenotypic plasticity: prolonged interaction between M1 macrophages and fibroblasts within the 3D microenvironment may induce partial repolarization toward a more pro-fibrotic state over time. Pro-inflammatory cytokines such as IL-6 and IL-1β are known to activate the JAK/STAT pathway, which can facilitate fibroblast-to-myofibroblast transformation (FMT) through non-canonical mechanisms.[15]

Additionally, activated myofibroblasts may reciprocally secrete TGF-β, which could repolarize M1 toward an M2-like phenotype via paracrine signaling, establishing a positive feedback loop that amplifies ECM production at later time points.[22]

CD86, immunostaining used as an M1 polarization marker, showed limited signal at the tested dilution of 1:50 and required further optimization. While CD68-positive macrophage presence was confirmed across all co-culture conditions, the specific M1 polarization state could not be conclusively validated by IHC within the 3D ring sections at this time. The persistence of a pro-inflammatory phenotype throughout the 7-day culture period remains to be confirmed, and alternative assays such as bulk RT-qPCR for M1-associated transcripts (e.g., CD86, IL6, TNF) or flow cytometry for surface expression should be incorporated in future experiments.

M1 co-cultured rings displayed prolonged αSMA-positive signaling through day 7, in contrast to M2 co-culture conditions and myofibroblast-only controls, which showed declining αSMA fluorescence over the same period. This sustained myofibroblast activation marker is consistent with the delayed increase in collagen production observed in M1 conditions and supports the hypothesis that M1 macrophages drive a temporally extended FMT process. The mechanism may involve chronic JAK/STAT activation downstream of IL-6 and IL-1β, which sustains fibroblast activation independent of, or cooperatively with, the canonical TGF-β/SMAD2/3 pathway.[15,22]

To validate the hypothesis of M1-to-M2 phenotypic repolarization over time, extended culture beyond day 7 with periodic supernatant collection and IHC/IF phenotyping will be conducted. Additionally, bulk RT-qPCR or flow cytometry at multiple time points would provide mechanistic insight into transcriptional changes associated with M1/M2 repolarization in the fibrotic microenvironment.

M2a Macrophage Co-culture

M2a co-culture rings started with the highest *x, y*-thickness values comparable to other mono- and co-culture conditions at very early time points. However, the tissue contracted from day 2 below basal mono-culture (fibroblast only). Among co-cultured groups, M2a maintained relatively greater thickness compared to M1 and M2c rings throughout the study. Day 7 *z*-dimensional analysis revealed that M2a co-culture produced thickness values similar to those of fibroblast-only rings, suggesting ECM synthesis in *z*-dimension. The *x, y*- and *z*-dimensional behavior in M2a rings is particularly interesting that M2a macrophages may have distinct spatial axes by reflecting anisotropic matrix deposition or directional contractile forces within the ring geometry towards the gel peg.

M2a co-culture rings produced the highest P1CP levels among all fibroblast co-culture conditions from day 2 onward, consistent with the well-established profibrotic role of M2a macrophages. M2a macrophages secrete TGF-β, which activates the canonical TGF-β/SMAD2/3 signaling pathway in fibroblasts to promote FMT and excessive ECM deposition. The early elevation in P1CP levels suggests that M2a-derived paracrine signaling rapidly activates collagen synthesis in co-cultured fibroblasts. This early profibrotic process may reflect M2a that predominates during intermediate-later stage of inflammation than that of other M2 subtypes.[23]

The gradual decline in P1CP concentration toward day 7, however, may reflect the onset of fibroblast dedifferentiation or feedback inhibition of the SMAD pathway in the absence of sustained polarization stimuli. However, the CD206 signal was not reliably detected in time-dependent 3D ring cryosections. Given macrophages' high phenotypic plasticity, the loss of M2a polarization markers over the culture period cannot be excluded and represents an important biological question for future investigation and needs to be validated on 2D monoculture.

Additional titration of CD206 positive signals compared to negative secondary antibody only staining needs to be conducted.

M2a co-cultured rings displayed elevated αSMA signals at early time points relative to the fibroblast-only negative control, consistent with profibrotic characteristic inducing TGF-β-mediated FMT promotion.[2,7] However, αSMA fluorescence declined toward day 7, mirroring the trajectory of collagen production and suggesting that myofibroblast activation is transient in this system without continuous profibrotic stimulation. This pattern may reflect M2a depolarized back to steady state M0 due to lack of continuous IL-4 stimulus over the 7-day culture period, or it may indicate a feedback-regulated decrease in fibroblast responsiveness to TGF-β over time. Also, Peng H. et al demonstrated that IL-4 is mediated by STAT6 pathway via IL-4Rα, the profibrotic process could be mediated by suppressed IL-4 stimulation.[24]

Future studies should investigate whether periodic re-stimulation with IL-4 or supplementation of TGF-β in the culture medium sustains M2a polarization and prolongs myofibroblast activation and collagen production. The M2a-myofibroblast co-culture result in which M2a unexpectedly showed the lowest collagen production suggests repolarization of M2a to serve as regulatory anti-fibrotic macrophages. Therefore, further studies of immunophenotyping, relative gene expressions, and downstream pathway activation should be analyzed.

M2c Macrophage Co-culture

M2c co-culture rings exhibited *x, y*-thickness values most similar to those of steady-state M0 macrophage conditions, suggesting that M2c macrophages exert a more moderate structural influence on the ring tissue compared to M1 or M2a phenotypes. This intermediate compaction behavior may reflect the distinct cytokine profile of M2c macrophages than that of another profibrotic macrophage, M2a.

M2c co-culture rings showed a delayed increase in P1CP concentration, with elevated collagen levels detected from day 4 onward, in contrast to M2a, which showed elevation from day 2. This temporal delay in collagen production may be attributable to the predominantly IL-10-mediated signaling of M2c macrophages which serves as an anti-inflammatory cytokine, which becomes profibrotic in prolonged existence.[25] Together, these findings suggest that M2c macrophages promote fibrogenesis through a more temporally delayed but sustained signaling mechanism.

CD163 immunostaining, used as the M2c polarization marker, was not reliably detected in time-dependent 3D ring cryosections similar to CD206. Optimization through increasing the primary antibody concentration and longer incubations of each antibody staining needs to be done. Also, as with M2a, phenotypic drift of M2c macrophages over the 7-day co-culture period should be considered as a potential confounding factor.

M2c co-cultured rings showed early αSMA activation above the fibroblast-only negative control, consistent with TGF-β-mediated promotion of FMT characteristic, but activation declined toward day 7, paralleling M2a behavior. This declining pattern, alongside the delayed P1CP increase, suggests that M2c macrophages may initiate but not sustain myofibroblast activation over the 7-day observation window. This is mechanistically plausible given that IL-10,

the primary M2c cytokine, has documented immunosuppressive effects that may limit the positive feedback amplification of fibrogenic signaling over time.

In the future, comparative cytokine profiling of M2c ring supernatants including IL-10 and TGF-β quantification at each time point would allow correlation of secreted factors with observed structural and biochemical changes. Additionally, since M2c macrophages are considered relevant to fibrosis resolution in some contexts, future experiments could explore whether their presence modulates responsiveness to anti-fibrotic compounds in this 3D platform.

Limitations

The 1:16 macrophage-to-fibroblast ratio adopted in this study was informed by a prior 3D spheroid co-culture study by Tan et al. in which M1 macrophages derived from peripheral blood mononuclear cells (PBMCs) were co-cultured with dermal fibroblasts across multiple ratios. In that study, the 1:16 ratio demonstrated the most pronounced pro-fibrotic response compared to other ratios tested, supporting its selection as a physiologically relevant condition for modeling fibrogenesis. However, it is important to note that the macrophage source in Tan et al. differed from the present study. PBMC-derived macrophages retain proliferative capacity, whereas THP-1 monocyte-derived macrophages used here are non-proliferating, which may result in a progressive shift in the effective macrophage-to-fibroblast ratio over the culture period due to fibroblast proliferation.[16]

Similarly, Lyu et al. employed a sessile drop array-based 3D multicellular co-culture system incorporating macrophages and fibroblasts at a 1:100 ratio, determined through optimization for feasible spheroid formation.[26] The substantially lower macrophage proportion in that system highlights that the optimal cellular ratio is highly context-dependent, varying with the culture platform, cell source, and the biological question being addressed.

Despite these prior studies, there remains a notable gap in the literature regarding scaffold-free 3D co-culture systems specifically designed to model macrophage-fibroblast interactions in the context of fibrosis. Most existing models rely on 2D monolayers, conditioned medium transfer, or scaffold-based hydrogels that do not fully recapitulate direct cell-cell contact in a 3D microenvironment. Advanced single-cell RNA sequencing (scRNA-seq) data representing spatial cellular populations within fibrotic foci have demonstrated that elevated

macrophage numbers are associated with fibrosis progression.[27] However, the specific macrophage subpopulation composition and their precise numerical proportions relativity vary across organ types and have not yet been comprehensively mapped. Therefore, the identification of an optimal macrophage-to-fibroblast ratio that accurately recapitulates the physiological microenvironment of each organ-specific fibrotic niche warrants further systematic investigation.

Conclusion

Fibrosis remains a significant clinical challenge due to its progressive and irreversible nature, which lacks curative therapies. In this study, we successfully developed a novel scaffold-free 3D ring-shaped co-culture platform that better recapitulates the complex fibrotic microenvironment compared to traditional 2D systems or 3D spheroids. This novel *in vitro* platform provides a multifactorial platform for future studies of fibrosis. By initial optimization of culture conditions, we identified a macrophage-to-fibroblast ratio of 1:16 in 50:50 serum-free media as the most stable and viable condition for ring formation. This condition provided robust tissue architecture while maintaining sufficient cell viability until day 7. These findings establish a practical and reproducible platform for studying macrophage-fibroblast crosstalk in a controlled 3D environment.

Our results also demonstrated phenotype-dependent differences in fibrogenic behavior. In particular, M1 macrophages were associated with sustained myofibroblast activation and increased collagen production at later time points, suggesting that pro-inflammatory signals may contribute to chronic fibroblast activation and to repolarization into M2 via a positive feedback loop involving myofibroblast secretion of TGF-β. M2a macrophages showed the highest early collagen-related activity, consistent with a profibrotic function, while M2c macrophages appeared to exhibit a comparatively more regulatory or resolving phenotype. Together, these findings highlight the importance of macrophage phenotype and temporal context in shaping fibroblast activation and fibrogenic outcomes.

Although additional validation, including bulk RT-qPCR and extended phenotypic characterization, is still needed to define the underlying signaling mechanisms, this 3D ring model provides a robust and versatile platform for fibrosis research. Its scaffold-free design

allows investigation of cell-cell interaction, tissue morphology, and mechanical behavior in a physiologically relevant setting. In the future, this model may be further applied to study mechanotransduction through tissue stretching (wound assay), to evaluate RNA interference and drug delivery, and to explore immune cell-driven mechanisms of fibrosis by the addition of Th cells or circulating monocytes. Overall, this platform offers a promising *in vitro* tool for bridging the gap between preclinical studies and clinical applications in fibrosis research, as an alternative to animal testing.

Supplementary Data

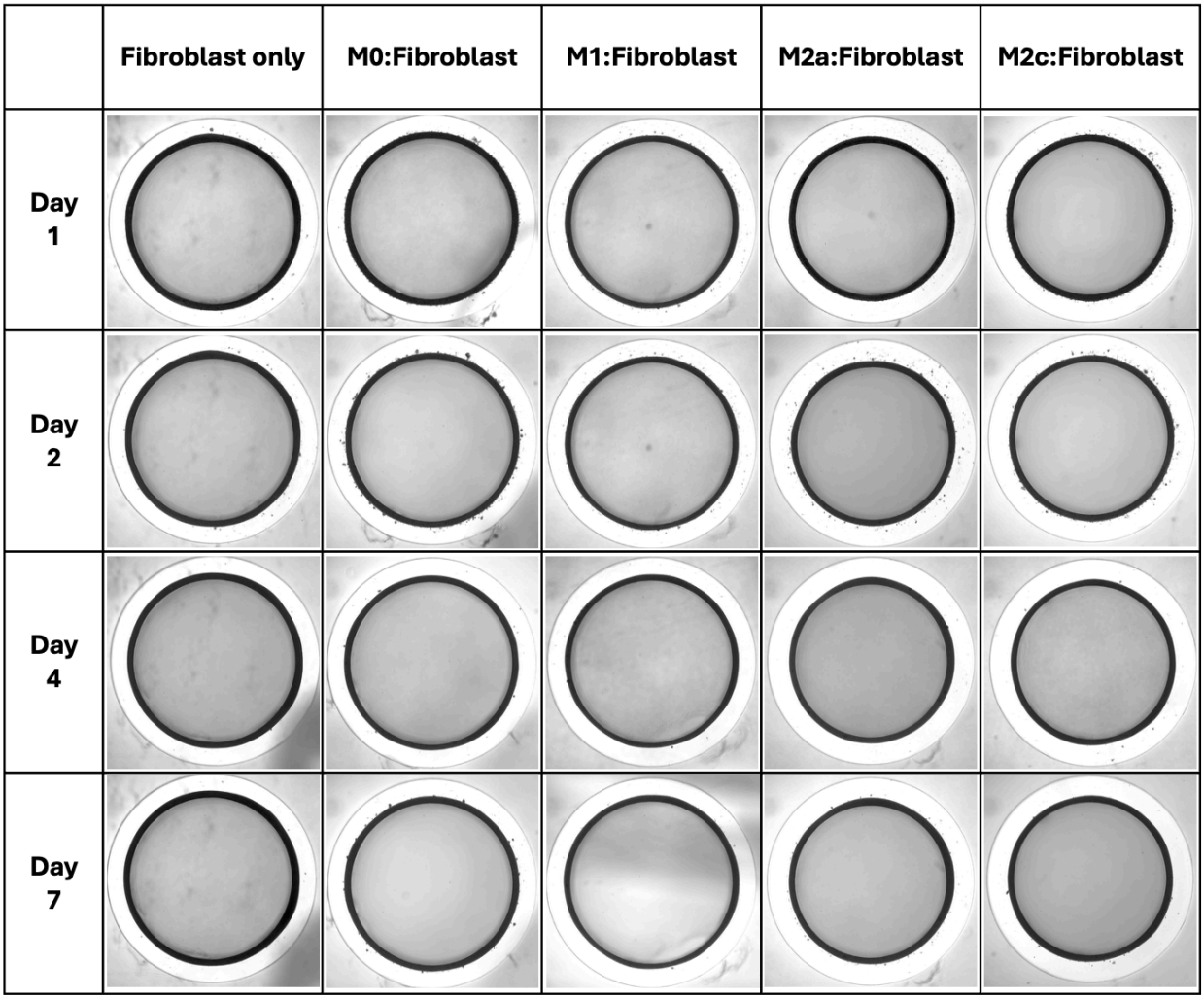

Figure S1. Brightfield images of 1:16 macrophage-to-fibroblasts co-culture rings over time. Bottom-view images of rings were acquired using a Nikon Eclipse Ts2 microscope at 2x magnification on day 1, 2, 4, and 7 (top to bottom). Columns represent different macrophage polarization phenotypes (M0, M1, M2a, M2c) co-cultured with fibroblasts at a 1:16 ratio, with fibroblast-only cultures as a negative control.

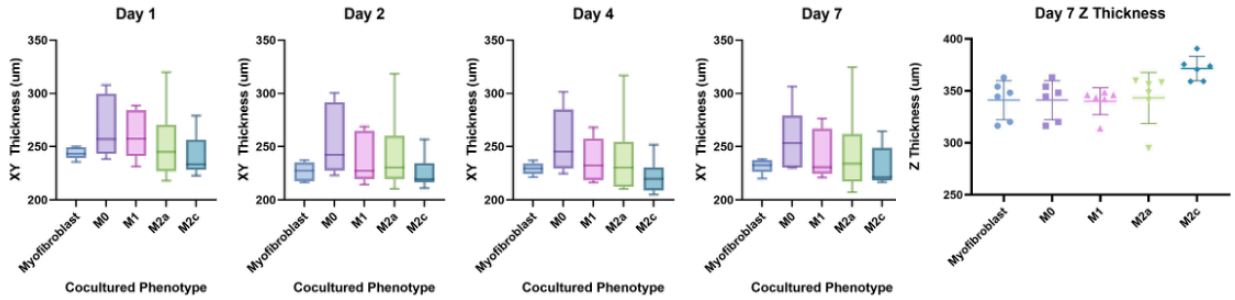

Figure S2. *x, y*-, and *z*-thickness measurements and statistical analysis on each macrophage phenotype-myofibroblast 1:16 co-culture rings.
x, y-dimensional thickness measured on 5x bottom view brightfield images taken on day 1, 2, 4, and 7. An average of 1,000 measurements per ring, totaling 6 rings per group, were analyzed. 20 *z*-dimensional thickness was measured on day 7 rings (n=6). Each dot indicates the average thickness per ring. Due to high variance, the thickness across groups was not statistically significant.

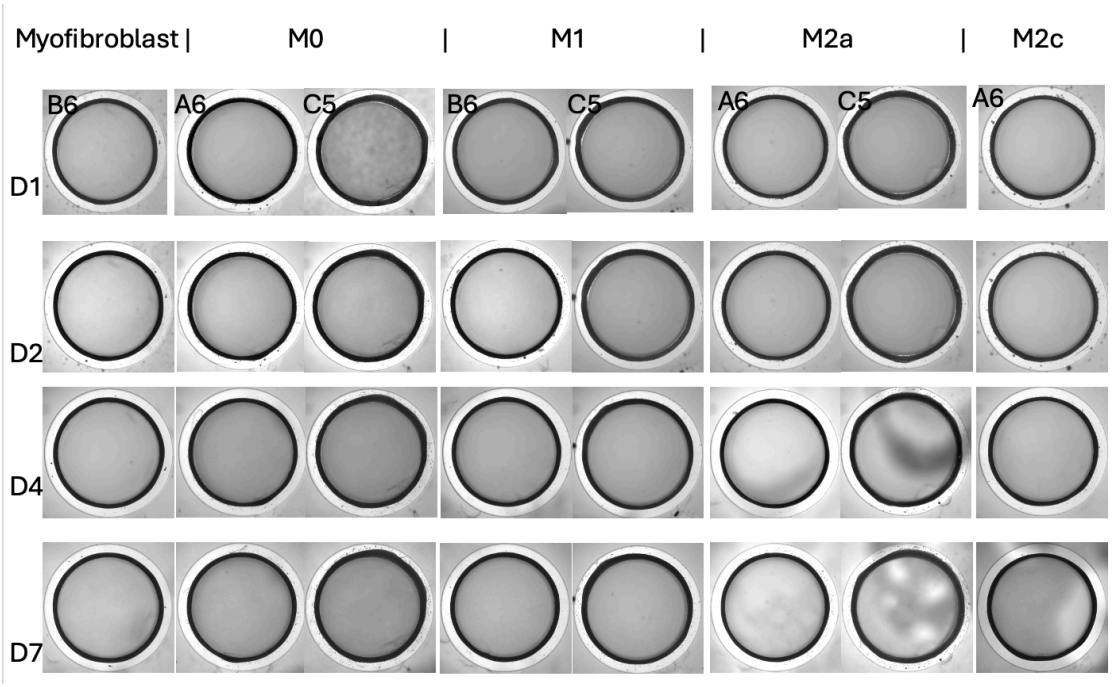

Figure S3. *x, y*-dimensional image of each macrophage phenotype to myofibroblasts. Bottom view under brightfield 5x microscopic images of myofibroblast only and M0, M1, M2a, and M2c with myofibroblast at 1:16 co-culture. 1 or 2 rings were periodically taken on day 1, 2, 4, and 7. M0, M1, and M2a ring images on the left are uniformly fabricated rings, while images on the right are rings that had puffed morphology.

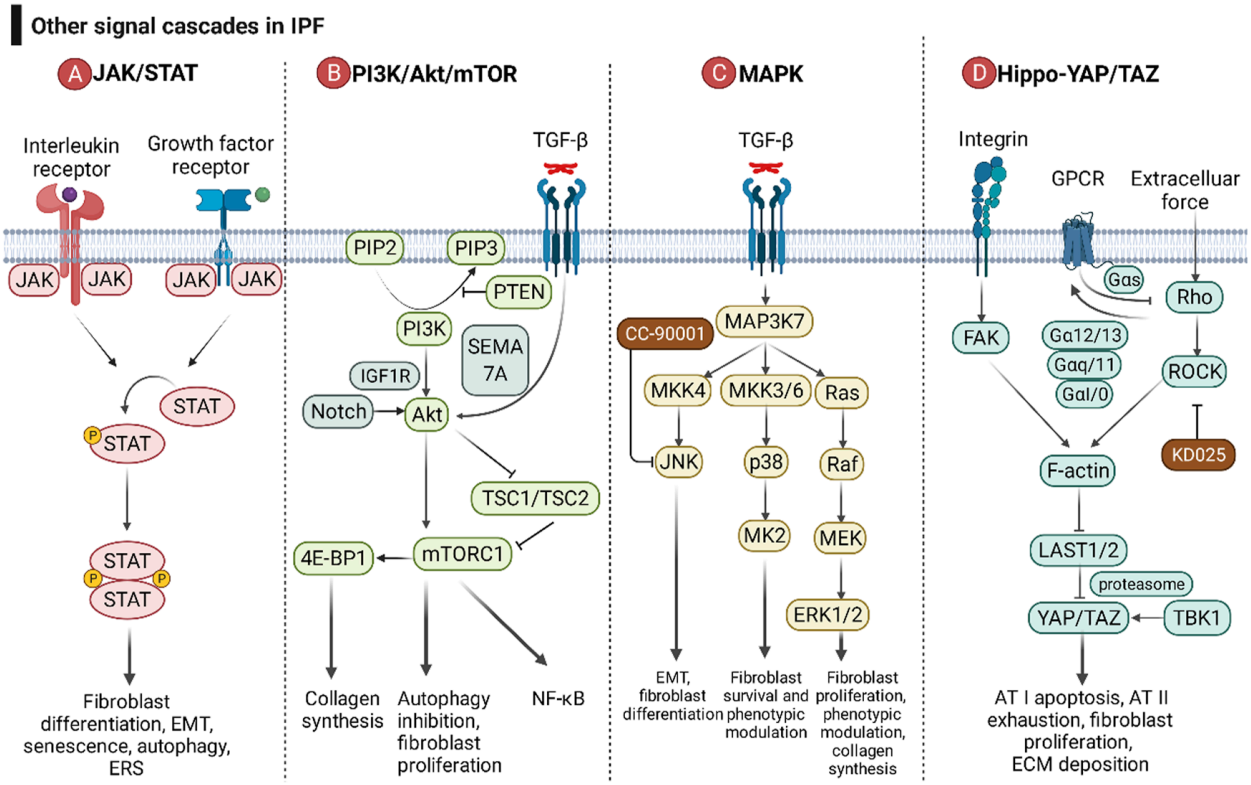

Figure S4. Non-canonical signaling pathway involved in fibrogenesis.
Schematic image demonstrates **(A)** JAK/STAT pathway, **(B)** PI3K/Akt/mTOR pathway, **(C)** MAPK pathway, and **(D)** Hippo-YAP/TAZ pathway that are investigated for profibrotic pathways for idiopathic pulmonary fibrosis.[15]

References

1. Deng Q, Wu L, Zhang C, Dang M. Global Fibrosis Burden and a Transcriptional Biomarker-Based Strategy for Early Detection in Resource-Limited Settings. *Biomolecules*. 2025;15(9):1273. doi:10.3390/biom15091273

2. Zhao M, Wang L, Wang M, et al. Targeting fibrosis: mechanisms and clinical trials. *Sig Transduct Target Ther*. 2022;7(1):206. doi:10.1038/s41392-022-01070-3

3. Mutsaers HAM, Merrild C, Nørregaard R, Plana-Ripoll O. The impact of fibrotic diseases on global mortality from 1990 to 2019. *J Transl Med*. 2023;21:818. doi:10.1186/s12967-023-04690-7

4. Antar SA, Ashour NA, Marawan ME, Al-Karmalawy AA. Fibrosis: Types, Effects, Markers, Mechanisms for Disease Progression, and Its Relation with Oxidative Stress, Immunity, and Inflammation. *Int J Mol Sci*. 2023;24(4):4004. doi:10.3390/ijms24044004

5. Koudstaal T, Wijsenbeek MS. Idiopathic pulmonary fibrosis. *La Presse Médicale*. 2023;52(3):104166. doi:10.1016/j.lpm.2023.104166

6. Borthwick LA, Wynn TA, Fisher AJ. Cytokine mediated tissue fibrosis. *Biochim Biophys Acta*. 2013;1832(7):1049-1060. doi:10.1016/j.bbadis.2012.09.014

7. Pakshir P, Noskovicova N, Lodyga M, et al. The myofibroblast at a glance. *J Cell Sci*. 2020;133(13):jcs227900. doi:10.1242/jcs.227900

8. Kreuter M, Lee JS, Tzouvelekis A, et al. Monocyte Count as a Prognostic Biomarker in Patients with Idiopathic Pulmonary Fibrosis. *Am J Respir Crit Care Med*. 2021;204(1):74-81. doi:10.1164/rccm.202003-0669OC

9. Kamiya M, Carter H, Espindola MS, et al. Immune mechanisms in fibrotic interstitial lung disease. *Cell*. 2024;187(14):3506-3530. doi:10.1016/j.cell.2024.05.015

10. Lis-López L, Bauset C, Seco-Cervera M, Cosín-Roger J. Is the Macrophage Phenotype Determinant for Fibrosis Development? *Biomedicines*. 2021;9(12):1747. doi:10.3390/biomedicines9121747

11. Mia S, Warnecke A, Zhang XM, Malmström V, Harris RA. An optimized Protocol for Human M2 Macrophages using M-CSF and IL-4/IL-10/TGF-β Yields a Dominant Immunosuppressive Phenotype. *Scandinavian Journal of Immunology*. 2014;79(5):305-314. doi:10.1111/sji.12162

12. Shi X, Young CD, Zhou H, Wang XJ. Transforming Growth Factor-β Signaling in Fibrotic Diseases and Cancer-Associated Fibroblasts. *Biomolecules*. 2020;10(12):1666. doi:10.3390/biom10121666

13. Henderson NC, Rieder F, Wynn TA. Fibrosis: from mechanisms to medicines. *Nature*. 2020;587(7835):555-566. doi:10.1038/s41586-020-2938-9

14. Chen F, Lyu L, Xing C, et al. The pivotal role of TGF-β/Smad pathway in fibrosis pathogenesis and treatment. *Front Oncol*. 2025;15:1649179. doi:10.3389/fonc.2025.1649179

15. Ma H, Liu S, Li S, Xia Y. Targeting Growth Factor and Cytokine Pathways to Treat Idiopathic Pulmonary Fibrosis. *Front Pharmacol*. 2022;13. doi:10.3389/fphar.2022.918771

16. Tan Y, Suarez A, Garza M, Khan AA, Elisseeff J, Coon D. Human fibroblast-macrophage tissue spheroids demonstrate ratio-dependent fibrotic activity for in vitro fibrogenesis model development. *Biomater Sci*. 2020;8(7):1951-1960. doi:10.1039/c9bm00900k

17. Ma H, Zhu M, Chen M, Li X, Feng X. The role of macrophage plasticity in neurodegenerative diseases. *Biomark Res*. 2024;12(1):81. doi:10.1186/s40364-024-00624-7

18. Zhou B wen, Liu H man, Xu F, Jia X hua. The role of macrophage polarization and cellular crosstalk in the pulmonary fibrotic microenvironment: a review. *Cell Commun Signal*. 2024;22:172. doi:10.1186/s12964-024-01557-2

19. Bankhead P, Loughrey MB, Fernández JA, et al. QuPath: Open source software for digital pathology image analysis. *Sci Rep*. 2017;7(1):16878. doi:10.1038/s41598-017-17204-5

20. Wilks BT, Evans EB, Nakhla MN, Morgan JR. Directing fibroblast self-assembly to fabricate highly-aligned, collagen-rich matrices. *Acta Biomaterialia*. 2018;81:70-79. doi:10.1016/j.actbio.2018.09.030

21. Tung NTC, Nogami M, Iwasaki M, et al. M2-like macrophages derived from THP-1 cells promote myofibroblast differentiation of synovial fibroblasts in association with the TGF-β1/SMAD2/3 signaling pathway. *Scientific Reports*. 2025;15(1):25505. doi:10.1038/s41598-025-10858-6

22. Denton CP, Ong VH, Xu S, et al. Therapeutic interleukin-6 blockade reverses transforming growth factor-beta pathway activation in dermal fibroblasts: insights from the faSScinate clinical trial in systemic sclerosis. *Annals of the Rheumatic Diseases*. 2018;77(9):1362-1371. doi:10.1136/annrheumdis-2018-213031

23. Novak CM, Sethuraman S, Luikart KL, et al. Alveolar macrophages drive lung fibroblast function in cocultures of IPF and normal patient samples. *American Journal of Physiology-Lung Cellular and Molecular Physiology*. 2023;324(4):L507-L520. doi:10.1152/ajplung.00263.2022

24. Peng H, Sarwar Z, Yang XP, et al. Profibrotic Role for Interleukin-4 in Cardiac Remodeling and Dysfunction. *Hypertension*. 2015;66(3):582-589. doi:10.1161/HYPERTENSIONAHA.115.05627

25. Sun L, Louie MC, Vannella KM, et al. New concepts of IL-10-induced lung fibrosis: fibrocyte recruitment and M2 activation in a CCL2/CCR2 axis. *American Journal of*

Physiology-Lung Cellular and Molecular Physiology. 2011;300(3):L341-L353. doi:10.1152/ajplung.00122.2010

26. Lyu X, Cui F, Zhou H, et al. 3D co-culture of macrophages and fibroblasts in a sessile drop array for unveiling the role of macrophages in skin wound-healing. *Biosens Bioelectron*. 2023;225:115111. doi:10.1016/j.bios.2023.115111

27. Su R, Song L, Liu Y, et al. Macrophage–Fibroblast Crosstalk in Fibrosis: Key Regulator of Fibrosis Across Different Organs. *Front Biosci (Landmark Ed)*. 2025;30(11). doi:10.31083/FBL38864